PHYSICAL REVIEW D **93,** 095021 (2016)

Quark flavor violating Higgs boson decay $h \to \bar{b}s + b\bar{s}$ in the MSSM

M. E. Gómez,[1,*] S. Heinemeyer,[2,3,†] and M. Rehman[2,‡]

[1]*Department of Applied Physics, University of Huelva, 21071 Huelva, Spain*
[2]*Instituto de Física de Cantabria (CSIC-UC), E-39005 Santander, Spain*
[3]*Instituto de Física Teórica, (UAM/CSIC), Universidad Autónoma de Madrid, Cantoblanco, E-28049 Madrid, Spain*

(Received 3 December 2015; published 26 May 2016)

We study the quark flavor violating Higgs boson decay $h \to \bar{b}s + b\bar{s}$ in the minimal supersymmetric standard model (MSSM). The decay is analyzed first in a model-independent approach and second in the minimal flavor violating (MFV) constrained MSSM. The experimental constraints from B-physics observables (BPO) and electroweak precision observables (EWPO) are also calculated and imposed on the parameter space. It is shown that, in some cases, the EWPO restrict the flavor violating parameter space more than the BPO. In the model-independent analysis, values of $\mathcal{O}(10^{-4})$ can be found for $\mathrm{BR}(h \to \bar{b}s + b\bar{s})$. In the MFV constrained MSSM (CMSSM), such results can only be obtained in very restricted parts of the parameter space. The results show that observation of the decay $h \to \bar{b}s + b\bar{s}$ in the MSSM at future e^+e^- colliders is not excluded.

DOI: 10.1103/PhysRevD.93.095021

I. INTRODUCTION

Supersymmetry (SUSY) is one of the most intriguing ideas from the last 30 years of high- energy physics. One of the major goals of the Large Hadron Collider (LHC) and future colliders is to discover SUSY [or any other sign of physics beyond the standard model (SM)]. As with other BSM models, this search for SUSY particles has thus far been unsuccessful. Another way to learn about SUSY is to study the indirect effects of the SUSY particles on SM observables. Flavor changing neutral current (FCNC) processes offer a unique prospective in this regard. In the SM, FCNC processes are absent at tree level and can only occur at one-loop level. The only source of FCNCs in the SM is the Cabibbo-Kobayashi-Maskawa (CKM) matrix, and these processes are highly suppressed due to Glashow-Iliopoulos-Maiani (GIM) cancellations [1]. On the other hand, in the MSSM [2], possible misalignment between the quark and scalar quark mass matrices is another source which can dominate the SM contribution by several orders of magnitude. Any possible experimental deviation from the SM prediction for FCNSs would be clear evidence of new physics and potentially a hint for MSSM.

Within the MSSM, flavor mixing can occur in the scalar fermion sector due to the possible presence of soft SUSY-breaking parameters in the respective mass matrices, which are off-diagonal in flavor space (mass parameters as well as trilinear couplings). This yields many new sources of flavor (and $\mathcal{CP}$) violation, which potentially lead to large nonstandard effects in flavor processes in conflict with experimental bounds from low-energy flavor observables involving strange, charm, or bottom mesons [3]. An elegant way to solve the above problems (in general BSM models) is provided by the minimal flavor violation (MFV) hypothesis [4,5], where flavor (and $\mathcal{CP}$) violation is assumed to originate entirely from the CKM matrix. For example, in the MSSM, the off-diagonality in the sfermion mass matrix reflects the misalignment (in flavor space) between fermion and sfermion mass matrices that cannot be diagonalized simultaneously. One way to introduce this misalignment within the MSSM under the MFV hypothesis is the following: Assuming no flavor violation at the grand unification (GUT) scale, off-diagonal sfermion mass matrix entries can be generated by renormalization group equations (RGE) running to the electroweak (EW) scale due to the presence of nondiagonal Yukawa matrices in RGEs. In this paper, we will take into account both possibilities: the general parametrization of flavor violation at the EW scale, as well as flavor violation induced only by CKM effects in the RGE running from the GUT to the EW scale.

MFV sceneraios are well motivated by the fact that low-energy meson physics puts tight constraints on the possible value of the FCNC couplings, especially for the first- and second-generation squarks which are sensitive to the data on $K^0 - \bar{K}^0$ and $D^0 - \bar{D}^0$ mixing. However, the third generation is less constrained, since present data on $B^0 - \bar{B}^0$ mixing still leave some room for FCNCs. This allows some parameter space for the more general scenarios focusing on the mixing between second- and third-generation (s)quarks. One such example is the neutral Higgs decay $h \to \bar{b}s + b\bar{s}$. The SM contribution is highly suppressed for this process but the SUSY-QCD quark-squark-gluino loop contribution can enhance the MSSM contribution by several orders of

*mario.gomez@dfa.uhu.es
†Sven.Heinemeyer@cern.ch
‡rehman@ifca.unican.es

magnitude. Also the SUSY-EW one-loop contribution from quark-squark-chargino and quark-squark-neutralino loop, even though subdominant, can have sizable effects on the $\mathrm{BR}(h \to \bar{b}s + b\bar{s})$, where in particular the interference effects of SUSY-QCD and SUSY-EW loop corrections can be relevant. This decay in the framework of the MSSM has been analyzed in the literature: the SUSY-QCD contributions for this decay were calculated in [6,7], and the SUSY-EW contributions using the mass insertion approximation were calculated in [8]. Later in [9] the SUSY-EW contributions and their interference effects with the SUSY-QCD contribution were calculated using exact diagonalization of the squark mass matrices. In all these analyses, only LL mixing (see below for an exact definition) in the squarks mass matrix was considered, and experimental constraints were imposed only from $\mathrm{BR}(B \to X_s\gamma)$. Most recently, in [10] RR mixing also has been included. However, mixing of the LR or RL elements of the mass matrix and constraints from other B-physics observables (BPO) or potential other constraints were not taken into account (except in the most recent analysis in [10]).

In this paper, we will analyze the decay $h \to \bar{b}s + b\bar{s}$, evaluated at the full one-loop level, by taking into account the experimental constraints not only from B-physics observables but also from the EWPO. In the scalar quark sector, we will not only consider the LL mixing, but also include the LR-RL and RR mixing for our analysis of $\mathrm{BR}(h \to \bar{b}s + b\bar{s})$. We will analyze this decay first in a model-independent approach (MI) where flavor-mixing parameters are put in by hand without any emphasis on the origin of this mixing (but respecting the experimental bounds from BPO and EWPO). In a second step, we perform the analysis in the MFV constrained MSSM (CMSSM), where flavor mixing is generated by the RGE running from the GUT down to the electroweak scale.

The paper is organized as follows: First, we review the main features of the MFV CMSSM and flavor mixing in the MSSM in Sec. II. The details about the calculation and computational setup of the low-energy observables are given in Sec. III. The numerical results are presented in Sec. IV, where first we show the MI analysis, followed by the results in MFV CMSSM. Our conclusions can be found in Sec. V.

II. MODEL SETUP

In this section, we will first briefly review the MSSM and parametrization of sfermion mixing at low energy. Subsequently, we will give a brief recap of the CMSSM and the concept of MFV.

A. Flavor mixing in the MSSM

In this section, we give a brief description about how we parametrize flavor mixing at the EW scale. We are using the same notation as in Refs. [11–15].

The most general hypothesis for flavor mixing assumes mass matrices for the scalar quarks (we ignore flavor mixing in the slepton sector) that are not diagonal in flavor space. The superfields are rotated such that quark matrices are diagonal. The rotation is performed via the CKM matrix, and the relevant terms in the soft SUSY-breaking Lagrangian (to be defined below) get rotated from the interaction eigenstate basis to what is known as the super-CKM basis.

In the squarks sector, we have two 6×6 mass matrices, based on the corresponding six super-CKM eigenstates, $\tilde{U}_{L,R}$ with $U = u, c, t$ for up-type squarks and $\tilde{D}_{L,R}$ with $D = d, s, b$ for down-type squarks.

The nondiagonal entries in these 6×6 general matrices for squarks can be described in terms of a set of dimensionless parameters δ_{ij}^{FAB} ($F = Q, U, D$; $A, B = L, R$; $i, j = 1, 2, 3$, $i \neq j$) where F identifies the squark type, L and R refer to the left- and right-handed SUSY partners of the corresponding fermionic degrees of freedom, and i, j indexes run over the three generations.

One usually writes the 6×6 nondiagonal mass matrices, $\mathcal{M}_{\tilde{u}}^2$ and $\mathcal{M}_{\tilde{d}}^2$, referred to in the super-CKM basis, being ordered, respectively, as $(\tilde{u}_L, \tilde{c}_L, \tilde{t}_L, \tilde{u}_R, \tilde{c}_R, \tilde{t}_R)$, $(\tilde{d}_L, \tilde{s}_L, \tilde{b}_L, \tilde{d}_R, \tilde{s}_R, \tilde{b}_R)$ and writes them in terms of left- and right-handed blocks $M_{\tilde{q}AB}^2$ ($q = u, d$, $A, B = L, R$), which are nondiagonal 3×3 matrices,

$$\mathcal{M}_{\tilde{q}}^2 = \begin{pmatrix} M_{\tilde{q}LL}^2 & M_{\tilde{q}LR}^2 \\ M_{\tilde{q}LR}^{2\dagger} & M_{\tilde{q}RR}^2 \end{pmatrix}, \qquad \tilde{q} = \tilde{u}, \tilde{d}, \tag{1}$$

where

$$\begin{aligned}
M_{\tilde{u}LLij}^2 &= m_{\tilde{U}_L ij}^2 + (m_{u_i}^2 + (T_3^u - Q_u s_{\mathrm{w}}^2) M_Z^2 \cos 2\beta)\delta_{ij}, \\
M_{\tilde{u}RRij}^2 &= m_{\tilde{U}_R ij}^2 + (m_{u_i}^2 + Q_u s_{\mathrm{w}}^2 M_Z^2 \cos 2\beta)\delta_{ij}, \\
M_{\tilde{u}LRij}^2 &= \langle \mathcal{H}_2^0 \rangle \mathcal{A}_{ij}^u - m_{u_i} \mu \cot\beta \delta_{ij}, \\
M_{\tilde{d}LLij}^2 &= m_{\tilde{D}_L ij}^2 + (m_{d_i}^2 + (T_3^d - Q_d s_{\mathrm{w}}^2) M_Z^2 \cos 2\beta)\delta_{ij}, \\
M_{\tilde{d}RRij}^2 &= m_{\tilde{D}_R ij}^2 + (m_{d_i}^2 + Q_d s_{\mathrm{w}}^2 M_Z^2 \cos 2\beta)\delta_{ij}, \\
M_{\tilde{d}LRij}^2 &= \langle \mathcal{H}_1^0 \rangle \mathcal{A}_{ij}^d - m_{d_i} \mu \tan\beta \delta_{ij},
\end{aligned} \tag{2}$$

with, $i, j = 1, 2, 3$, $Q_u = 2/3$, $Q_d = -1/3$, $T_3^u = 1/2$ and $T_3^d = -1/2$. $M_{Z,W}$ denote the Z and W boson masses, with $s_{\mathrm{w}}^2 = 1 - M_W^2/M_Z^2$, and $(m_{u_1}, m_{u_2}, m_{u_3}) = (m_u, m_c, m_t)$, $(m_{d_1}, m_{d_2}, m_{d_3}) = (m_d, m_s, m_b)$ are the quark masses. μ is the Higgsino mass term and $\tan\beta = v_2/v_1$ with $v_1 = \langle \mathcal{H}_1^0 \rangle$ and $v_2 = \langle \mathcal{H}_2^0 \rangle$ being the two vacuum expectation values of the corresponding neutral Higgs boson in the Higgs $SU(2)_L$ doublets, $\mathcal{H}_1 = (\mathcal{H}_1^0 \mathcal{H}_1^-)$ and $\mathcal{H}_2 = (\mathcal{H}_2^+ \mathcal{H}_2^0)$.

It should be noted that the nondiagonality in flavor comes exclusively from the soft SUSY-breaking parameters

that could be nonvanishing for $i \neq j$, namely, the masses $m^2_{\tilde{U}_L ij}$, $m^2_{\tilde{U}_R ij}$, $m^2_{\tilde{D}_L ij}$, $m^2_{\tilde{D}_R ij}$ and the trilinear couplings, $\mathcal{A}^q_{ij}$.

It is important to note that, due to $SU(2)_L$ gauge invariance, the same soft masses $m_{\tilde{Q}ij}$ enter in both up-type and down-type squark mass matrices. The soft SUSY-breaking parameters for the up-type squarks differ from corresponding ones for down-type squarks by a rotation with the CKM matrix. The sfermion mass matrices in terms of the δ^{FAB}_{ij} are given as

$$m^2_{\tilde{U}_L} = \begin{pmatrix} m^2_{\tilde{Q}_1} & \delta^{QLL}_{12} m_{\tilde{Q}_1} m_{\tilde{Q}_2} & \delta^{QLL}_{13} m_{\tilde{Q}_1} m_{\tilde{Q}_3} \\ \delta^{QLL}_{21} m_{\tilde{Q}_2} m_{\tilde{Q}_1} & m^2_{\tilde{Q}_2} & \delta^{QLL}_{23} m_{\tilde{Q}_2} m_{\tilde{Q}_3} \\ \delta^{QLL}_{31} m_{\tilde{Q}_3} m_{\tilde{Q}_1} & \delta^{QLL}_{32} m_{\tilde{Q}_3} m_{\tilde{Q}_2} & m^2_{\tilde{Q}_3} \end{pmatrix}, \tag{3}$$

$$m^2_{\tilde{D}_L} = V^\dagger_{\mathrm{CKM}} m^2_{\tilde{U}_L} V_{\mathrm{CKM}}, \tag{4}$$

$$m^2_{\tilde{U}_R} = \begin{pmatrix} m^2_{\tilde{U}_1} & \delta^{URR}_{12} m_{\tilde{U}_1} m_{\tilde{U}_2} & \delta^{URR}_{13} m_{\tilde{U}_1} m_{\tilde{U}_3} \\ \delta^{URR}_{21} m_{\tilde{U}_2} m_{\tilde{U}_1} & m^2_{\tilde{U}_2} & \delta^{URR}_{23} m_{\tilde{U}_2} m_{\tilde{U}_3} \\ \delta^{URR}_{31} m_{\tilde{U}_3} m_{\tilde{U}_1} & \delta^{URR}_{32} m_{\tilde{U}_3} m_{\tilde{U}_2} & m^2_{\tilde{U}_3} \end{pmatrix}, \tag{5}$$

$$m^2_{\tilde{D}_R} = \begin{pmatrix} m^2_{\tilde{D}_1} & \delta^{DRR}_{12} m_{\tilde{D}_1} m_{\tilde{D}_2} & \delta^{DRR}_{13} m_{\tilde{D}_1} m_{\tilde{D}_3} \\ \delta^{DRR}_{21} m_{\tilde{D}_2} m_{\tilde{D}_1} & m^2_{\tilde{D}_2} & \delta^{DRR}_{23} m_{\tilde{D}_2} m_{\tilde{D}_3} \\ \delta^{DRR}_{31} m_{\tilde{D}_3} m_{\tilde{D}_1} & \delta^{DRR}_{32} m_{\tilde{D}_3} m_{\tilde{D}_2} & m^2_{\tilde{D}_3} \end{pmatrix}, \tag{6}$$

$$v_2 \mathcal{A}^u = \begin{pmatrix} m_u A_u & \delta^{ULR}_{12} m_{\tilde{Q}_1} m_{\tilde{U}_2} & \delta^{ULR}_{13} m_{\tilde{Q}_1} m_{\tilde{U}_3} \\ \delta^{ULR}_{21} m_{\tilde{Q}_2} m_{\tilde{U}_1} & m_c A_c & \delta^{ULR}_{23} m_{\tilde{Q}_2} m_{\tilde{U}_3} \\ \delta^{ULR}_{31} m_{\tilde{Q}_3} m_{\tilde{U}_1} & \delta^{ULR}_{32} m_{\tilde{Q}_3} m_{\tilde{U}_2} & m_t A_t \end{pmatrix}, \tag{7}$$

$$v_1 \mathcal{A}^d = \begin{pmatrix} m_d A_d & \delta^{DLR}_{12} m_{\tilde{Q}_1} m_{\tilde{D}_2} & \delta^{DLR}_{13} m_{\tilde{Q}_1} m_{\tilde{D}_3} \\ \delta^{DLR}_{21} m_{\tilde{Q}_2} m_{\tilde{D}_1} & m_s A_s & \delta^{DLR}_{23} m_{\tilde{Q}_2} m_{\tilde{D}_3} \\ \delta^{DLR}_{31} m_{\tilde{Q}_3} m_{\tilde{D}_1} & \delta^{DLR}_{32} m_{\tilde{Q}_3} m_{\tilde{D}_2} & m_b A_b \end{pmatrix}. \tag{8}$$

Throughout this work, for simplicity, we are assuming that all δ^{FAB}_{ij} parameters are real; therefore, the Hermiticity of $\mathcal{M}^2_{\tilde{q}}$ implies $\delta^{FAB}_{ij} = \delta^{FBA}_{ji}$, and only the entries on and above the diagonal need to be filled. The δ^{FAB}_{ij} are located at the following places in the mass matrix:

$$\left(\begin{array}{ccc|ccc} \cdot & \delta^{FLL}_{12} & \delta^{FLL}_{13} & \cdot & \delta^{FLR}_{12} & \delta^{FLR}_{13} \\ \cdot & \cdot & \delta^{FLL}_{23} & \delta^{FRL*}_{12} & \cdot & \delta^{FLR}_{23} \\ \cdot & \cdot & \cdot & \delta^{FRL*}_{13} & \delta^{FRL*}_{23} & \cdot \\ \hline \cdot & \cdot & \cdot & \cdot & \delta^{FRR}_{12} & \delta^{FRR}_{13} \\ \cdot & \cdot & \cdot & \cdot & \cdot & \delta^{FRR}_{23} \\ \cdot & \cdot & \cdot & \cdot & \cdot & \cdot \end{array}\right)$$

The next step is to rotate the squark states from the super-CKM basis, $\tilde{q}_{L,R}$, to the physical basis. If we set the order in the super-CKM basis as above, $(\tilde{u}_L, \tilde{c}_L, \tilde{t}_L, \tilde{u}_R, \tilde{c}_R, \tilde{t}_R)$ and $(\tilde{d}_L, \tilde{s}_L, \tilde{b}_L, \tilde{d}_R, \tilde{s}_R, \tilde{b}_R)$, and in the physical basis as $\tilde{u}_{1,..6}$ and $\tilde{d}_{1,..6}$, respectively, these last rotations are given by two 6×6 matrices, $R^{\tilde{u}}$ and $R^{\tilde{d}}$,

$$\begin{pmatrix} \tilde{u}_1 \\ \tilde{u}_2 \\ \tilde{u}_3 \\ \tilde{u}_4 \\ \tilde{u}_5 \\ \tilde{u}_6 \end{pmatrix} = R^{\tilde{u}} \begin{pmatrix} \tilde{u}_L \\ \tilde{c}_L \\ \tilde{t}_L \\ \tilde{u}_R \\ \tilde{c}_R \\ \tilde{t}_R \end{pmatrix}, \qquad \begin{pmatrix} \tilde{d}_1 \\ \tilde{d}_2 \\ \tilde{d}_3 \\ \tilde{d}_4 \\ \tilde{d}_5 \\ \tilde{d}_6 \end{pmatrix} = R^{\tilde{d}} \begin{pmatrix} \tilde{d}_L \\ \tilde{s}_L \\ \tilde{b}_L \\ \tilde{d}_R \\ \tilde{s}_R \\ \tilde{b}_R \end{pmatrix}, \tag{9}$$

yielding the diagonal mass-squared matrices for squarks as follows,

$$\mathrm{diag}\{m^2_{\tilde{u}_1}, m^2_{\tilde{u}_2}, m^2_{\tilde{u}_3}, m^2_{\tilde{u}_4}, m^2_{\tilde{u}_5}, m^2_{\tilde{u}_6}\} = R^{\tilde{u}} \mathcal{M}^2_{\tilde{u}} R^{\tilde{u}\dagger}, \tag{10}$$

$$\mathrm{diag}\{m^2_{\tilde{d}_1}, m^2_{\tilde{d}_2}, m^2_{\tilde{d}_3}, m^2_{\tilde{d}_4}, m^2_{\tilde{d}_5}, m^2_{\tilde{d}_6}\} = R^{\tilde{d}} \mathcal{M}^2_{\tilde{d}} R^{\tilde{d}\dagger}. \tag{11}$$

B. The CMSSM and MFV

The MSSM is the simplest supersymmetric structure we can build from the SM particle content [2]. Following the notation of [16], its superpotential can be written as

$$\begin{aligned} \mathcal{W}_{\mathrm{MSSM}} = \epsilon_{ab}[&(Y_E)_{ij} \hat{\mathcal{H}}^a_1 \hat{\mathcal{L}}^b_i \hat{\mathcal{E}}_j + (Y_D)_{ij} \hat{\mathcal{H}}^a_1 \hat{\mathcal{Q}}^b_i \hat{\mathcal{D}}_j \\ &+ (Y_U)_{ij} \hat{\mathcal{H}}^b_2 \hat{\mathcal{Q}}^a_i \hat{\mathcal{U}}_j - \mu \hat{\mathcal{H}}^a_1 \hat{\mathcal{H}}^b_2], \end{aligned} \tag{12}$$

where the hats denote superfields, index i, $j = 1, 2, 3$ are generation indices, a, $b = 1, 2$ are $SU(2)$ indices, and ϵ is a completely antisymmetric 2×2 matrix, with $\epsilon_{12} = 1$. Matrices Y_E, Y_D, and Y_U are the Yukawa matrices.

The general setup for the soft SUSY-breaking parameters is given by

$$
\begin{aligned}
-\mathcal{L}_{\text{soft}} &= (m^2_{\tilde{Q}})_{ij}\tilde{\mathcal{Q}}^\dagger_i\tilde{\mathcal{Q}}_j + (m^2_{\tilde{U}})_{ij}\tilde{\mathcal{U}}^*_i\tilde{\mathcal{U}}_j + (m^2_{\tilde{D}})_{ij}\tilde{\mathcal{D}}^*_i\tilde{\mathcal{D}}_j \\
&+ (m^2_{\tilde{L}})_{ij}\tilde{\mathcal{L}}^\dagger_i\tilde{\mathcal{L}}_j + (m^2_{\tilde{E}})_{ij}\tilde{\mathcal{E}}^*_i\tilde{\mathcal{E}}_j + m^2_{H_1}\mathcal{H}^\dagger_1\mathcal{H}_1 \\
&+ m^2_{H_2}\mathcal{H}^\dagger_2\mathcal{H}_2 + \epsilon_{ab}[(\bar{A}^e)_{ij}\mathcal{H}^a_1\tilde{\mathcal{L}}^b_i\tilde{\mathcal{E}}^*_j \\
&+ (\bar{A}^d)_{ij}\mathcal{H}^a_1\tilde{\mathcal{Q}}^b_i\tilde{\mathcal{D}}^*_j + (\bar{A}^u)_{ij}\mathcal{H}^b_2\tilde{\mathcal{Q}}^a_i\tilde{\mathcal{U}}^*_j - B\mu\mathcal{H}^a_1\mathcal{H}^b_2] \\
&+ \left[\frac{1}{2}M_1\tilde{B}\,\tilde{B} + \frac{1}{2}M_2\tilde{W}^\alpha\tilde{W}^\alpha + \frac{1}{2}M_3\tilde{G}^\beta\tilde{G}^\beta + \text{H.c.}\right],
\end{aligned}
\tag{13}
$$

where the isospin and color indices α and β run over 1–3 and 1–8, respectively. Here we have used calligraphic capital letters for the sfermion fields in the interaction basis with generation indices,

$$
\begin{aligned}
&\tilde{\mathcal{U}}_{1,2,3} = \tilde{u}_R, \tilde{c}_R, \tilde{t}_R; \qquad \tilde{\mathcal{D}}_{1,2,3} = \tilde{d}_R, \tilde{s}_R, \tilde{b}_R; \\
&\tilde{\mathcal{Q}}_{1,2,3} = (\tilde{u}_L\tilde{d}_L)^T, (\tilde{c}_L\tilde{s}_L)^T, (\tilde{t}_L\tilde{b}_L)^T
\end{aligned}
\tag{14}
$$

$$
\begin{aligned}
&\tilde{\mathcal{E}}_{1,2,3} = \tilde{e}_R, \tilde{\mu}_R, \tilde{\tau}_R; \\
&\tilde{\mathcal{L}}_{1,2,3} = (\tilde{\nu}_{eL}\tilde{e}_L)^T, (\tilde{\nu}_{\mu L}\tilde{\mu}_L)^T, (\tilde{\nu}_{\tau L}\tilde{\tau}_L)^T.
\end{aligned}
\tag{15}
$$

In accordance with Sec. II A, $m^2_{\tilde{Q}}$ and $m^2_{\tilde{L}}$ are 3×3 matrices in family space (with i, j being the generation indices) for the soft masses of the left-handed squark $\tilde{\mathcal{Q}}$ and slepton $\tilde{\mathcal{L}}$ $SU(2)$ doublets, respectively. $m^2_{\tilde{U}}$, $m^2_{\tilde{D}}$, and $m^2_{\tilde{E}}$ contain the soft masses for right-handed up-type squark $\tilde{\mathcal{U}}$, down-type squarks $\tilde{\mathcal{D}}$ and charged slepton $\tilde{\mathcal{E}}$ $SU(2)$ singlets, respectively. $\bar{A}^u$, $\bar{A}^d$, and $\bar{A}^e$ are the 3×3 matrices for the trilinear couplings for up-type squarks, down-type squarks, and charged slepton, respectively. m_{H_1} and m_{H_2} contain the soft masses of the Higgs sector. In the last line, M_1, M_2, and M_3 define the bino, wino, and gluino mass terms, respectively; see Eqs. (7), (8).

Within the CMSSM, the soft SUSY-breaking parameters are assumed to be universal at the grand unification scale $M_{\text{GUT}} \sim 2\times 10^{16}$ GeV,

$$
\begin{aligned}
&(m^2_{\tilde{Q}})_{ij} = (m^2_{\tilde{U}})_{ij} = (m^2_{\tilde{D}})_{ij} = (m^2_{\tilde{L}})_{ij} = (m^2_{\tilde{E}})_{ij} = m^2_0\delta_{ij}, \\
&m^2_{H_1} = m^2_{H_2} = m^2_0, \\
&m_{\tilde{g}} = m_{\tilde{W}} = m_{\tilde{B}} = m_{1/2}, \\
&(\bar{A}^u)_{ij} = A_0 e^{i\phi_A}(Y_U)_{ij}, \qquad (\bar{A}^d)_{ij} = A_0 e^{i\phi_A}(Y_D)_{ij}, \\
&(\bar{A}^e)_{ij} = A_0 e^{i\phi_A}(Y_E)_{ij}.
\end{aligned}
\tag{16}
$$

There is a common mass for all the scalars, m^2_0, a single gaugino mass, $m_{1/2}$, and all the trilinear soft-breaking terms are directly proportional to the corresponding Yukawa couplings in the superpotential with a proportionality constant $A_0 e^{i\phi_A}$, containing a potential nontrivial complex phase. The other phases can be redefined and included in the phase of μ (for a review, see for example [17]). However, they are very constrained by the electric dipole moments (EDMs) of leptons and nucleons [18].

With the use of the RGE of the MSSM, one can obtain the SUSY spectrum at the EW scale. All the SUSY masses and mixings are then given as a function of m^2_0, $m_{1/2}$, A_0, and $\tan\beta = v_2/v_1$, the ratio of the two vacuum expectation values (see below). We require radiative symmetry breaking to fix $|\mu|$ and $|B\mu|$ [19,20] with the tree-level Higgs potential.

By definition, this model fulfills the MFV hypothesis, since the only flavor violating terms stem from the CKM matrix. The important point is that, even in a model with universal soft SUSY-breaking terms at some high-energy scale as the CMSSM, some off-diagonality in the squark mass matrices appears at the EW scale. Working in the basis where the squarks are rotated parallel to the quarks, the so-called super CKM (SCKM) basis, the squark mass matrices are not flavor diagonal at the EW scale. This is due wto the fact that at M_{GUT} there exist two nontrivial flavor structures, namely the two Yukawa matrices for the up and down quarks, which are not simultaneously diagonalizable. This implies that through RGE evolution some flavor-mixing leaks into the sfermion mass matrices. In a general SUSY model, the presence of new flavor structures in the soft SUSY-breaking terms would generate large flavor mixing in the sfermion mass matrices. However, in the CMSSM, the two Yukawa matrices are the only source of flavor change. As always in the SCKM basis, any off-diagonal entry in the sfermion mass matrices at the EW scale will be necessarily proportional to a product of Yukawa couplings.

In Ref. [15], it was shown that, even under the MFV hypothesis in the CMSSM, non-negligible flavor violation effects can be induced at the EW scale. Confronted with precision data from flavor observables or electroweak precision observables, this can lead to important restrictions of the CMSSM parameter space. These constraints will be imposed on the SUSY parameters in our numerical analysis below. Details about these observables and their calculation are given in the next section.

III. LOW-ENERGY OBSERVABLES

Here we briefly describe the calculations of the observables evaluated in this work. We start with the evaluation of the flavor violating Higgs decay, $h \to \bar{b}s + b\bar{s}$, and then give a short description of the precision observables used to restrict the allowed parameter space.

A. The flavor violating Higgs decay $h \to \bar{b}s + b\bar{s}$

We start with the evaluation of the flavor violating Higgs decay. In the SM, the branching ratio $\text{BR}(h \to \bar{b}s + b\bar{s})$ can be at most of $\mathcal{O}(10^{-7})$ [6], too small to have a chance of detection at the LHC. But because of the strong FCNC gluino couplings and the $\tan\beta$ enhancement inherent to the

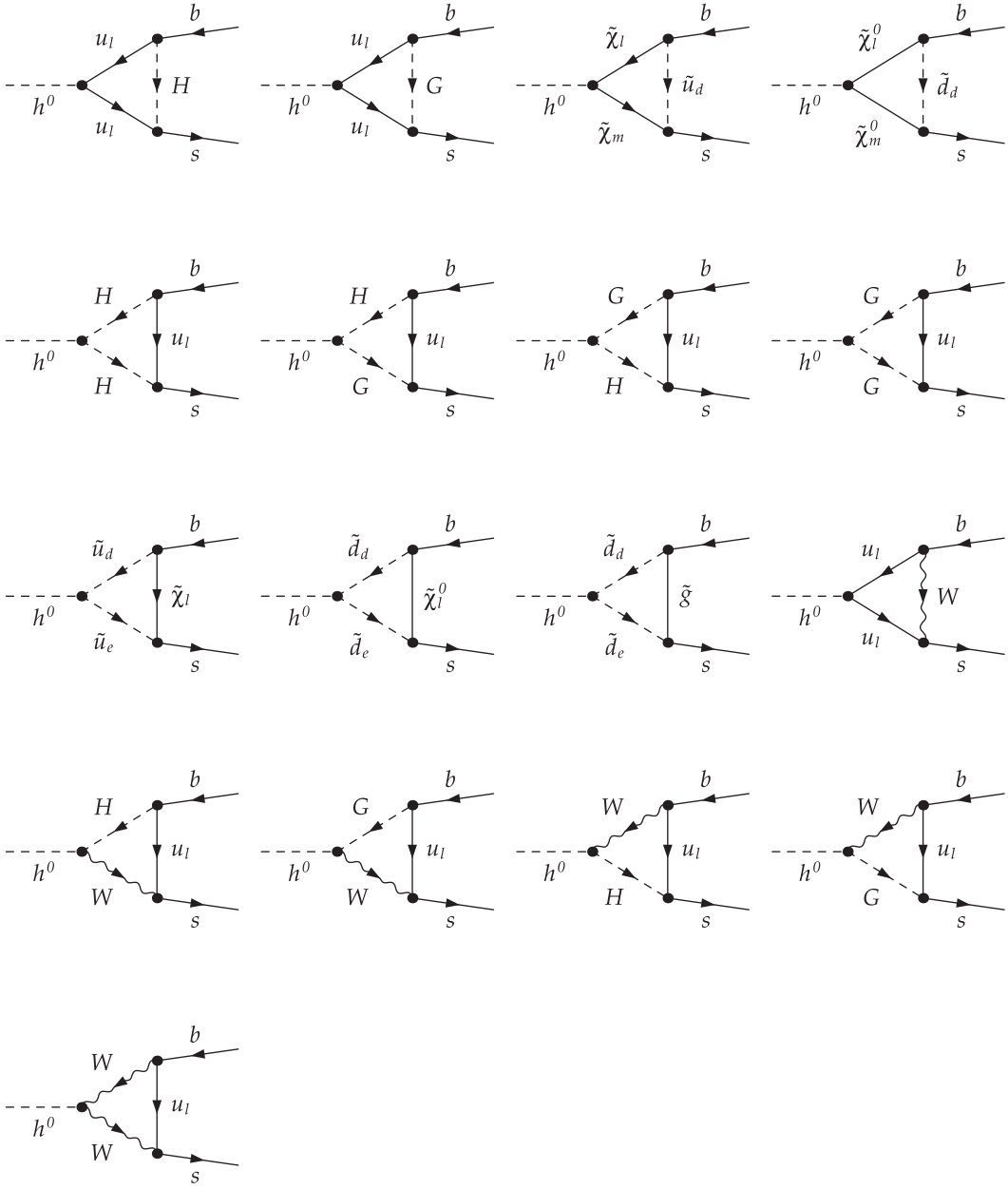

FIG. 1. Generic Feynman diagrams for the EW and QCD corrections to $h \to \bar{b}s + b\bar{s}$ (vertex diagrams).

MSSM Yukawa couplings, we may expect an increase of several orders of magnitude in the branching ratio as compared to the SM result; see Refs. [6,7]. We (re)calculate full one-loop contributions from SUSY-QCD as well as SUSY-EW loops with the help of the FeynArts [21,22] and FormCalc [23] packages. The lengthy analytical results are not shown here. We take into account mixing in the LL and RR part, as well as in the LR and RL part of the mass matrix, contrary to Refs. [6–10], where only the LL and RR mixing was considered. For our numerical analysis, we define

$$\mathrm{BR}(h \to \bar{b}s + b\bar{s}) = \frac{\Gamma(h \to \bar{b}s + b\bar{s})}{\Gamma^{\mathrm{MSSM}}_{h,\mathrm{tot}}}, \qquad (17)$$

where $\Gamma^{\mathrm{MSSM}}_{h,\mathrm{tot}}$ is the total decay width of the light Higgs boson h of the MSSM, as evaluated with FeynHiggs [24–28]. The contributing Feynman diagrams for the decay $h \to \bar{b}s + b\bar{s}$ are shown in Fig. 1 (vertex corrections) and in Fig. 2 (self-energy corrections).

Which BR might be detectable at the LHC or an e^+e^- collider such as the ILC can only be established by means of specific experimental analyses, which, to our knowledge, do not exist yet. However, in the literature, it is expected to measure BRs at the level of 10^{-3} at the LHC [6]. In the clean ILC environment, in general, Higgs boson branching ratios below the level of 10^{-4} can be observed; see e.g. Ref. [29] for a recent review. We will take this as a

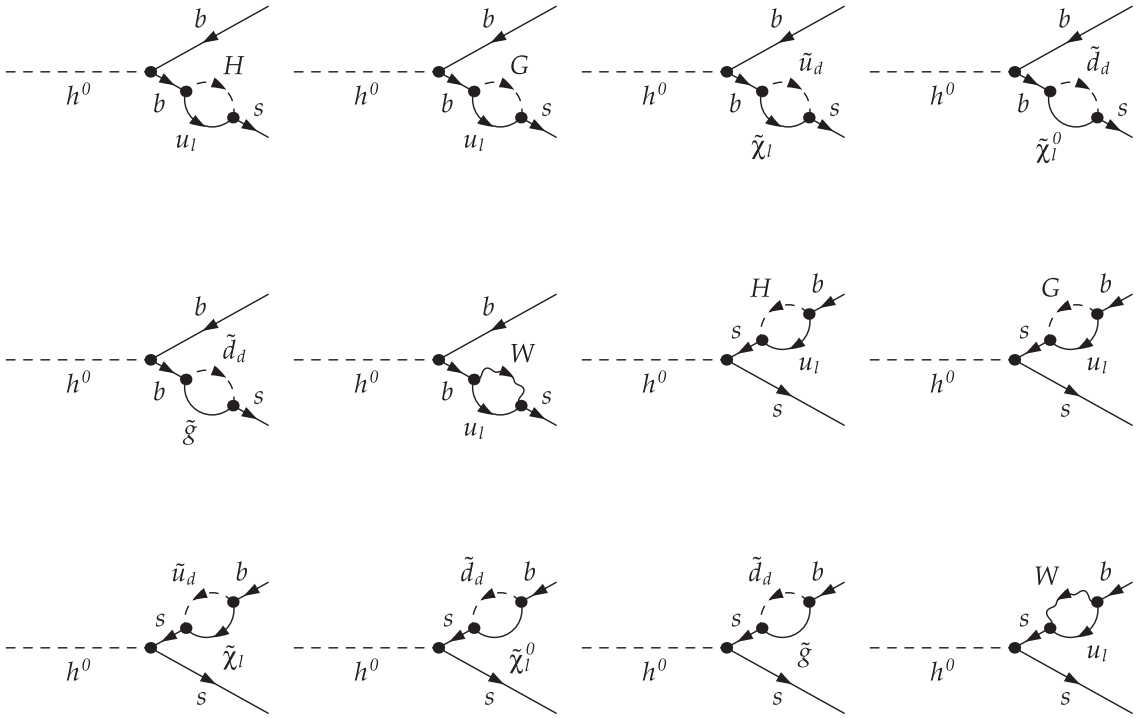

FIG. 2. Generic Feynman diagrams for the EW and QCD corrections to $h \to \bar{b}s + b\bar{s}$ (self-energy contributions).

rough guideline concerning the level at which the decay $h \to \bar{b}s + b\bar{s}$ could be observable.

B. B-physics observables

In order to determine which flavor mixing (i.e. which combination of parameters) is still allowed by experimental data, we evaluated flavor precision observables and electroweak precision observables. Here we start with the brief description of the evaluation of several B-physics observables (BPO): $\mathrm{BR}(B \to X_s\gamma)$, $\mathrm{BR}(B_s \to \mu^+\mu^-)$, and ΔM_{B_s}. Concerning $\mathrm{BR}(B \to X_s\gamma)$, included in the calculation are the most relevant loop contributions to the Wilson coefficients: (i) loops with Higgs bosons (including the resummation of large $\tan\beta$ effects [30]), (ii) loops with charginos, and (iii) loops with gluinos. For $\mathrm{BR}(B_s \to \mu^+\mu^-)$, there are three types of relevant one-loop corrections contributing to the relevant Wilson coefficients: (i) box diagrams, (ii) Z-penguin diagrams, and (iii) neutral Higgs boson ϕ-penguin diagrams, where ϕ denotes the three neutral MSSM Higgs bosons, $\phi = h$, H, A (again large resummed $\tan\beta$ effects have been taken into account). In our numerical evaluation, there are included what are known to be the dominant contributions to these three types of diagrams [31]: chargino contributions to box and Z-penguin diagrams and chargino and gluino contributions to ϕ-penguin diagrams. Concerning ΔM_{B_s}, in the MSSM there are in general three types of one-loop diagrams that contribute: (i) box diagrams, (ii) Z-penguin diagrams, and (iii) double Higgs-penguin diagrams (again including the resummation of large $\tan\beta$ enhanced effects). In our numerical evaluation, there are included again what are known to be the dominant contributions to these three types of diagrams in scenarios with nonminimal flavor violation (for a review, see, for instance, [32]): gluino contributions to box diagrams, chargino contributions to box and Z-penguin diagrams, and chargino and gluino contributions to double ϕ-penguin diagrams. More details about the calculations employed can be found in Refs. [13,14]. We perform our numerical calculation with the BPHYSICS subroutine taken from the SuFla code [33] (with some additions and improvements as detailed in Refs. [13,14]), which has been implemented as a subroutine into (a private version of) FeynHiggs. The experimental status and SM prediction of these observables are given in Table I [34–41][1]

C. Electroweak precision observables

Electroweak precision observables (EWPO) that are known with accuracy at the per-mille level or better have the potential to allow a discrimination between quantum effects of the SM and SUSY models; see Ref. [43] for a review. An example is the W-boson mass M_W, whose present experimental value is [44]

$$M_W^{\mathrm{exp,today}} = 80.385 \pm 0.015\ \mathrm{GeV}. \tag{18}$$

[1]Using the most up-to-date value of $\mathrm{BR}(B_s \to \mu^+\mu^-) = 2.9 \pm 0.7 \times 10^{-9}$ [42] would have had a minor impact on our analysis.

TABLE I. Present experimental status of B-physics observables with their SM prediction.

Observable	Experimental value	SM prediction
$\mathrm{BR}(B\to X_s\gamma)$	$3.43\pm0.22\times10^{-4}$	$3.15\pm0.23\times10^{-4}$
$\mathrm{BR}(B_s\to\mu^+\mu^-)$	$(3.0)^{+1.0}_{-0.9}\times10^{-9}$	$3.23\pm0.27\times10^{-9}$
ΔM_{B_s}	$116.4\pm0.5\times10^{-10}$ MeV	$(117.1)^{+17.2}_{-16.4}\times10^{-10}$ MeV

The experimental uncertainty will further be reduced [45] to

$$\delta M_W^{\mathrm{exp,future}} \lesssim 4 \text{ MeV} \tag{19}$$

at the ILC and at the GigaZ option of the ILC, respectively. Even higher precision could be expected from the FCC-ee; see, e.g., Ref. [46].

The W-boson mass can be evaluated from

$$M_W^2\left(1-\frac{M_W^2}{M_Z^2}\right)=\frac{\pi\alpha}{\sqrt{2}G_\mu}(1+\Delta r), \tag{20}$$

where α is the fine-structure constant and G_μ the Fermi constant. This relation arises from comparing the prediction for muon decay with the experimentally precisely known Fermi constant. The one-loop contributions to Δr can be written as

$$\Delta r=\Delta\alpha-\frac{c_\mathrm{w}^2}{s_\mathrm{w}^2}\Delta\rho+(\Delta r)_\mathrm{rem}, \tag{21}$$

where $\Delta\alpha$ is the shift in the fine-structure constant due to the light fermions of the SM, $\Delta\alpha\propto\log(M_Z/m_f)$, and $\Delta\rho$ is the leading contribution to the ρ parameter [47] from (certain) fermion and sfermion loops (see below). The remainder part $(\Delta r)_\mathrm{rem}$ contains, in particular, the contributions from the Higgs sector.

The SUSY contributions to M_W can be well approximated with the ρ-parameter approximation [43,48]. M_W is affected by shifts in the quantity $\Delta\rho$ according to

$$\Delta M_W\approx\frac{M_W}{2}\frac{c_\mathrm{w}^2}{c_\mathrm{w}^2-s_\mathrm{w}^2}\Delta\rho. \tag{22}$$

The quantity $\Delta\rho$ is defined by the relation

$$\Delta\rho=\frac{\Sigma_Z^\mathrm{T}(0)}{M_Z^2}-\frac{\Sigma_W^\mathrm{T}(0)}{M_W^2}, \tag{23}$$

with the unrenormalized transverse parts of the Z- and W-boson self-energies at zero momentum, $\Sigma_{Z,W}^\mathrm{T}(0)$. It represents the leading universal corrections to the electroweak precision observables induced by mass splitting between partners in isospin doublets [47]. Consequently, it is sensitive to the mass-splitting effects induced by flavor mixing. The effects from flavor violation in the squark and slepton sector, entering via $\Delta\rho$, have been evaluated in Refs. [11,15,48] and included in FeynHiggs. In particular, in Ref. [48] it has been shown that, for the squark contributions, $\Delta\rho$ constitutes an excellent approximation to Δr. We use FeynHiggs for our numerical evaluation, where M_W is evaluated as

$$M_W^\mathrm{MSSM}=M_W^\mathrm{SM}+\Delta M_W^\mathrm{MSSM}, \tag{24}$$

where ΔM_W^MSSM is calculated via Eq. (22). FeynHiggs takes into account the full set of one-loop squark contributions to $\Delta\rho$ (including NMFV effects [11,48]), as well as the leading gluonic two-loop corrections [49]. In Ref. [15], it was shown that EWPO and in particular M_W can lead to relevant restrictions on the (C)MSSM parameter space in the presence of intergenerational mixing in the squark sector.

The prediction of M_W also suffers from various kinds of theoretical uncertainties, parametric and intrinsic. Starting with the parametric uncertainties, an experimental error of 1 GeV on m_t yields a parametric uncertainty on M_W of about 6 MeV, while the parametric uncertainties induced by the current experimental error of the hadronic contribution to the shift in the fine-structure constant, $\Delta\alpha_\mathrm{had}$, and by the experimental error of M_Z amount to about 2 and 2.5 MeV, respectively. The uncertainty of the M_W prediction caused by the experimental uncertainty of the Higgs mass $\delta M_h^\mathrm{exp}\lesssim 0.3$ GeV is significantly smaller ($\approx$0.2 MeV). The parametric uncertainties are added in quadrature and yield a total parametric uncertainty of 6.8 MeV. The intrinsic uncertainties from unknown higher-order corrections in the case of no flavor mixing have been estimated to be around 4.7–9.4 MeV in the MSSM [50,51] depending on the SUSY mass scale, where we have adopted the smaller value corresponding to larger SUSY mass scales. We have added the parameteric intrinsic uncertainties linearly. On top of the "known" intrinsic uncertainties, which were derived under the assumption of no flavor violation, we assume additionally a 10% uncertainty from the flavor-mixing contribution to $\Delta\rho^\mathrm{MSSM}$ and [via Eq. (22)] and add it linearly to the other uncertainties. This latter uncertainty is a naive estimate of flavor-mixing effects at the two-loop level, where an additional factor $\mathcal{O}(\alpha_s)$ enters.

IV. NUMERICAL RESULTS

In this section, we present our numerical results. We start with the model-independent approach, where we do not specify the origin of the flavor violating δ_{ij}^{FAB} but take into account the existing limits from BPO and (evaluate newly the ones from) EWPO. In a second step, we briefly investigate the results in the CMSSM.

The largest effects are expected from the mixing of the third and second generation of squarks. In order to keep the

TABLE II. Selected points in the MSSM parameter space (upper part) and their corresponding spectra (lower part). All dimensionful quantities are in GeV.

	S1	S2	S3	S4	S5	S6
$m_{\tilde{L}_{1,2}}$	500	750	1000	800	500	1500
$m_{\tilde{L}_3}$	500	750	1000	500	500	1500
M_2	500	500	500	500	750	300
A_τ	500	750	1000	500	0	1500
μ	400	400	400	400	800	300
$\tan\beta$	20	30	50	40	10	40
M_A	500	1000	1000	1000	1000	1500
$m_{\tilde{Q}_{1,2}}$	2000	2000	2000	2000	2500	1500
$m_{\tilde{Q}_3}$	2000	2000	2000	500	2500	1500
A_t	2300	2300	2300	1000	2500	1500
$m_{\tilde{l}_{1\ldots6}}$	489–515	738–765	984–1018	474–802	488–516	1494–1507
$m_{\tilde{\nu}_{1\ldots3}}$	496	747	998	496–797	496	1499
$m_{\tilde{\chi}^\pm_{1,2}}$	375–531	376–530	377–530	377–530	710–844	247–363
$m_{\tilde{\chi}^0_{1\ldots4}}$	244–531	245–531	245–530	245–530	373–844	145–363
M_h	126.6	127.0	127.3	123.1	123.8	125.1
M_H	500	1000	999	1001	1000	1499
M_A	500	1000	1000	1000	1000	1500
$M_{H^\pm}$	507	1003	1003	1005	1003	1502
$m_{\tilde{u}_{1\ldots6}}$	1909–2100	1909–2100	1908–2100	336–2000	2423–2585	1423–1589
$m_{\tilde{d}_{1\ldots6}}$	1997–2004	1994–2007	1990–2011	474–2001	2498–2503	1492–1509
$m_{\tilde{g}}$	2000	2000	2000	2000	3000	1200

number of free parameters at a manageable level, in our numerical analysis we only investigate δ_{23}^{FAB}, while our analytical result allows any $\delta_{ij}^{FAB} \neq 0$.

A. Model-independent analysis

In the model-independent analysis, we first define our set of input paramters and discuss how they are restricted by BPO and EWPO introduced above. In the allowed parameter space, we evaluate $\mathrm{BR}(h \to \bar{b}s + b\bar{s})$ and show that it might be detectable at future e^+e^- colliders.

1. Input parameters

For the following numerical analysis, we chose the MSSM parameter sets of Ref. [11,12]. This framework contains six specific points S1…S6 in the MSSM parameter space, all of which are compatible with present experimental data, including LHC searches and the measurements of the muon anomalous magnetic moment. The values of the various MSSM parameters as well as the values of the predicted MSSM mass spectra are summarized in Table II. They were evaluated with the program FeynHiggs [24–28].

For simplicity, and to reduce the number of independent MSSM input parameters, we assume equal soft masses for the sleptons of the first and second generations (similarly for the squarks), and for the left and right slepton sectors (similarly for the squarks). We choose equal trilinear couplings for the stop and sbottom squarks and for the sleptons consider only the stau trilinear coupling; the others are set to zero. We assume an approximate GUT relation for the gaugino soft-SUSY-breaking parameters. The pseudoscalar Higgs mass M_A and the μ parameter are taken as independent input parameters. In summary, the six points S1…S6 are defined in terms of the following subset of ten input MSSM parameters:

$$
\begin{aligned}
&m_{\tilde{L}_1} = m_{\tilde{L}_2}, \qquad m_{\tilde{L}_3}, \qquad (\text{with} \quad m_{\tilde{L}_i} = m_{\tilde{E}_i}, i = 1,2,3)\\
&m_{\tilde{Q}_1} = m_{\tilde{Q}_2} \qquad m_{\tilde{Q}_3},\\
&\qquad (\text{with} \quad m_{\tilde{Q}_i} = m_{\tilde{U}_i} = m_{\tilde{D}_i}, i = 1,2,3)\\
&A_t = A_b, \qquad A_\tau,\\
&M_2 = 2M_1 = M_3/4, \qquad \mu,\\
&M_A, \qquad \tan\beta.
\end{aligned}
$$

The specific values of these ten MSSM parameters in Table II are chosen to provide different patterns in the various sparticle masses, but all leading to rather heavy spectra and thus naturally in agreement with the absence of SUSY signals at the LHC. In particular, all points lead to rather heavy squarks of the first and second generation and gluinos above 1500 GeV and heavy sleptons above 500 GeV (where the LHC limits would also permit substantially lighter sleptons). The values of M_A within the interval (500, 1500) GeV, $\tan\beta$ within the interval

(10,50) and a large A_t within (1000, 2500) GeV are fixed such that a light Higgs boson h within the LHC-favored range (123, 127) GeV is obtained.

The large values of $M_A \geq 500$ GeV place the Higgs sector of our scenarios in the so-called decoupling regime [52], where the couplings of h to gauge bosons and fermions are close to the SM Higgs couplings, and the heavy H couples like the pseudoscalar A, and all heavy Higgs bosons are close in mass. With increasing M_A, the heavy Higgs bosons tend to decouple from low-energy physics, and the light h behaves like the SM Higgs boson. This type of MSSM Higgs sector seems to be in good agreement with recent LHC data [53]. We checked with the code HiggsBounds [54] that this is indeed the case (although S3 is right "at the border").

In particular, the absence of gluinos at the LHC so far forbids too low M_3 and, through the assumed GUT relation, also a too low M_2. This is reflected by our choice of M_2 and μ which give gaugino masses compatible with present LHC bounds. Finally, we required that all our points lead to a prediction of the anomalous magnetic moment of the muon in the MSSM that can fill the present discrepancy between the SM prediction and the experimental value.

2. Experimental constraints on δ_{ij}^{FAB}

In this section, we will present the present experimental constraints on the squark-mixing parameters δ_{ij}^{FAB} for the above-mentioned MSSM points S1…S6 defined in Table II. The experimental constraints from BPO for the same set of parameters that we are using were already calculated in [14] for one $\delta_{ij}^{FAB} \neq 0$, which we reproduce here for completeness in Table III.

We now turn our attention to the constraints from M_W. In Fig. 3, we show the M_W as a function of δ_{23}^{QLL}, δ_{23}^{ULR}, and δ_{23}^{DLR} in the scenarios S1…S6. The area between the orange lines shows the allowed value of M_W with 3σ experimental uncertainty. The corresponding constraints from M_W on δ_{ij}^{FAB}, also taking into account the theoretical uncertainties as described at the end of Sec. III C, are shown in Table IV. No constraints can be found on the δ_{ij}^{RR}, as their contribution to M_W does not reach the MeV level, and consequently we do not show them here. Furthermore, the constraints on the δ_{23}^{URL} and δ_{23}^{DRL} are similar to that of δ_{23}^{ULR} and δ_{23}^{DLR}, respectively, and not shown here.

On the other hand, the constraints on δ_{23}^{QLL} are modified by the EWPO especially the region $(-0.83 : -0.78)$ for the point S5, which was allowed by the BPO, is now excluded. The allowed intervals for the points S1-S3 have also shrunk. However, the point S4 was already excluded by BPO; similarly, the allowed interval for S6 did not get modified by EWPO. The constraints on δ_{23}^{ULR} and δ_{23}^{DLR} are less restrictive than the ones from BPO except for the point S4 where the region $(0.076 : 0.12)$ is excluded for δ_{23}^{DLR} by EWPO.

TABLE III. Present allowed (by BPO) intervals for the squark-mixing parameters δ_{ij}^{FAB} for the selected S1-S6 MSSM points defined in Table II [14].

		Total allowed intervals
δ_{23}^{QLL}	S1	$(-0.27 : 0.28)$
	S2	$(-0.23 : 0.23)$
	S3	$(-0.12 : 0.06)$ $(0.17 : 0.19)$
	S4	excluded
	S5	$(-0.83 : -0.78)$ $(-0.14 : 0.14)$
	S6	$(-0.076 : 0.14)$
δ_{23}^{ULR}	S1	$(-0.27 : 0.27)$
	S2	$(-0.27 : 0.27)$
	S3	$(-0.27 : 0.27)$
	S4	excluded
	S5	$(-0.22 : 0.22)$
	S6	$(-0.37 : 0.37)$
δ_{23}^{DLR}	S1	$(-0.0069 : 0.014)$ $(0.12 : 0.13)$
	S2	$(-0.0069 : 0.014)$ $(0.11 : 0.13)$
	S3	$(-0.0069 : 0.014)$ $(0.11 : 0.13)$
	S4	$(0.076 : 0.12)$ $(0.26 : 0.30)$
	S5	$(-0.014 : 0.021)$ $(0.17 : 0.19)$
	S6	$(0 : 0.0069)$ $(0.069 : 0.076)$
δ_{23}^{URL}	S1	$(-0.27 : 0.27)$
	S2	$(-0.27 : 0.27)$
	S3	$(-0.27 : 0.27)$
	S4	excluded
	S5	$(-0.22 : 0.22)$
	S6	$(-0.37 : 0.37)$
δ_{23}^{DRL}	S1	$(-0.034 : 0.034)$
	S2	$(-0.034 : 0.034)$
	S3	$(-0.034 : 0.034)$
	S4	excluded
	S5	$(-0.062 : 0.062)$
	S6	$(-0.021 : 0.021)$
δ_{23}^{URR}	S1	$(-0.99 : 0.99)$
	S2	$(-0.99 : 0.99)$
	S3	$(-0.98 : 0.97)$
	S4	excluded
	S5	$(-0.99 : 0.99)$
	S6	$(-0.96 : 0.94)$
δ_{23}^{DRR}	S1	$(-0.96 : 0.96)$
	S2	$(-0.96 : 0.96)$
	S3	$(-0.96 : 0.94)$
	S4	excluded
	S5	$(-0.97 : 0.97)$
	S6	$(-0.97 : -0.94)$ $(-0.63 : 0.64)$ $(0.93 : 0.97)$

3. $\mathbf{BR}(h \to \bar{b}s + b\bar{s})$

In order to illustrate the contributions from different diagrams, we show in Fig. 4 the SUSY-EW, SUSY-QCD, and total SUSY contribution to $\Gamma(h \to \bar{b}s + b\bar{s})$ as a function of δ_{23}^{QLL} (upper left), δ_{23}^{DLR} (upper right), δ_{23}^{DRL} (lower left), and δ_{23}^{DRR} (lower right). These four δ_{ij}^{FAB} are the only relevant ones, since we are mainly concerned with the down-type sector, and mixing with the first generation does not play a role.

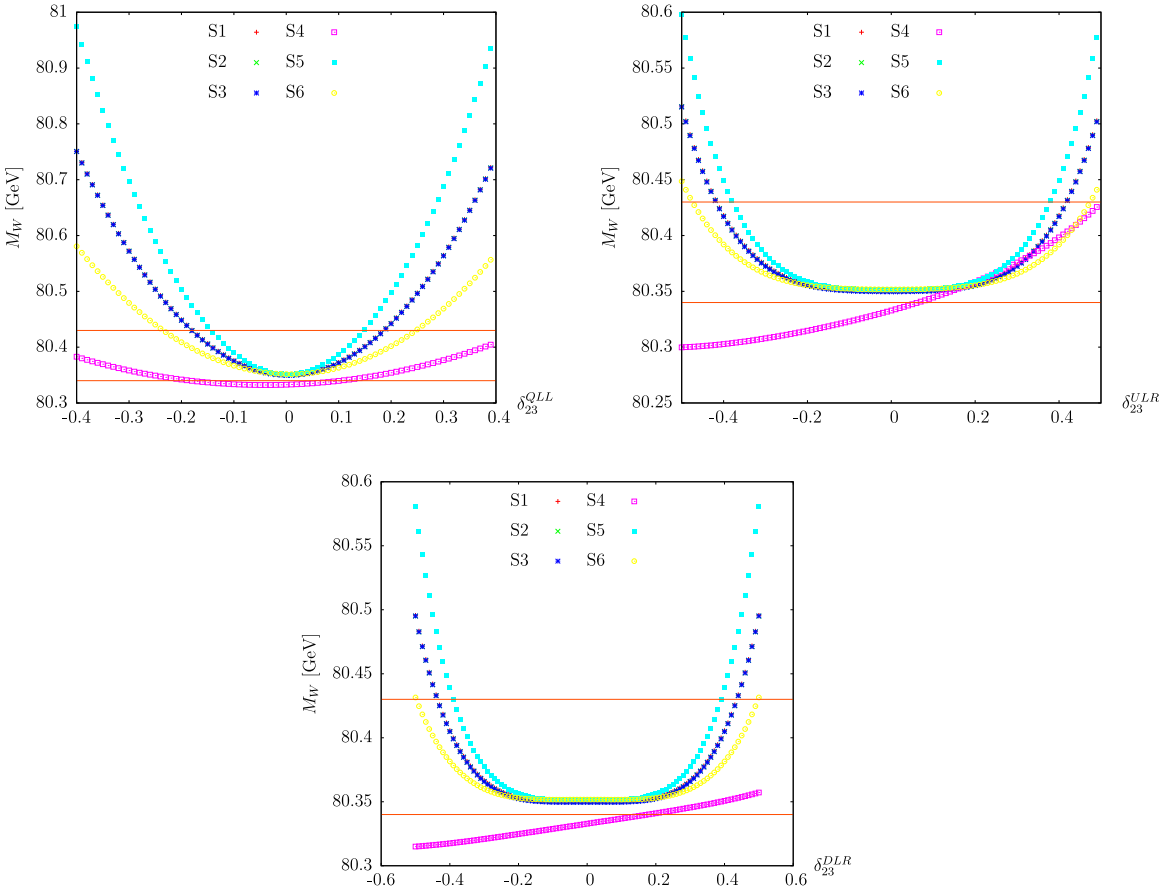

FIG. 3. M_W as a function of δ_{23}^{QLL} (upper left), δ_{23}^{ULR} (upper right), and δ_{23}^{DLR} (lower).

TABLE IV. Present allowed (by M_W) intervals for the squark-mixing parameters δ_{ij}^{FAB} for the selected S1-S6 MSSM points defined in Table II.

		Total allowed intervals
δ_{23}^{QLL}	S1	(−0.18 : 0.18)
	S2	(−0.18 : 0.18)
	S3	(−0.18 : 0.18)
	S4	(−0.53 : − 0.17) (0.10 : 0.45)
	S5	(−0.14 : 0.14)
	S6	(−0.23 : 0.23)
$\delta_{23}^{ULR}, \delta_{23}^{URL}$	S1	(−0.41 : 0.41)
	S2	(−0.41 : 0.41)
	S3	(−0.41 : 0.41)
	S4	(0.10 : 0.50)
	S5	(−0.39 : 0.39)
	S6	(−0.47 : 0.47)
$\delta_{23}^{DLR}, \delta_{23}^{DRL}$	S1	(−0.43 : 0.43)
	S2	(−0.43 : 0.43)
	S3	(−0.43 : 0.43)
	S4	(0.16 : 0.99)
	S5	(−0.39 : 0.39)
	S6	(−0.49 : 0.49)

In order to compare our results with the literature, we have used the same set of input parameters as in [9]

$$\mu = 800\,\text{GeV}, \quad m_{\text{SUSY}} = 800\,\text{GeV}, \quad A_f = 500\,\text{GeV},$$
$$M_A = 400\,\text{GeV}, \quad M_2 = 300\,\text{GeV}, \quad \tan\beta = 35, \qquad (25)$$

where we have chosen, for simplicity, m_{SUSY} as a common value for the soft SUSY-breaking squark mass parameters, $m_{\text{SUSY}} = M_{\tilde{Q},q} = M_{\tilde{U},(c,t)} = M_{\tilde{D},(s,b)}$, and all the various trilinear parameters to be universal, $A_f = A_t = A_b = A_c = A_s$. The value of the δ_{ij}^{FAB}'s are varied from −0.9 to 0.9, and GUT relations are used to calculate M_1 and M_3. In Ref. [9], only LL mixing was considered. In this limit, we find results in qualitative agreement with Ref. [9]. This analysis has been done just to illustrate the different contributions, and we do not take into account any experimental constraints. A detailed analysis for realistic SUSY scenarios (defined in Table II) constrained by BPO and EWPO can be found below.

As can be seen in Fig. 4, for the decay width $\Gamma(h \to \bar{b}s + b\bar{s})$ the SUSY-QCD contribution is dominant in all the cases. For LL mixing shown in the upper left plot, the SUSY-QCD contribution reaches up to $\mathcal{O}(10^{-6})$, while

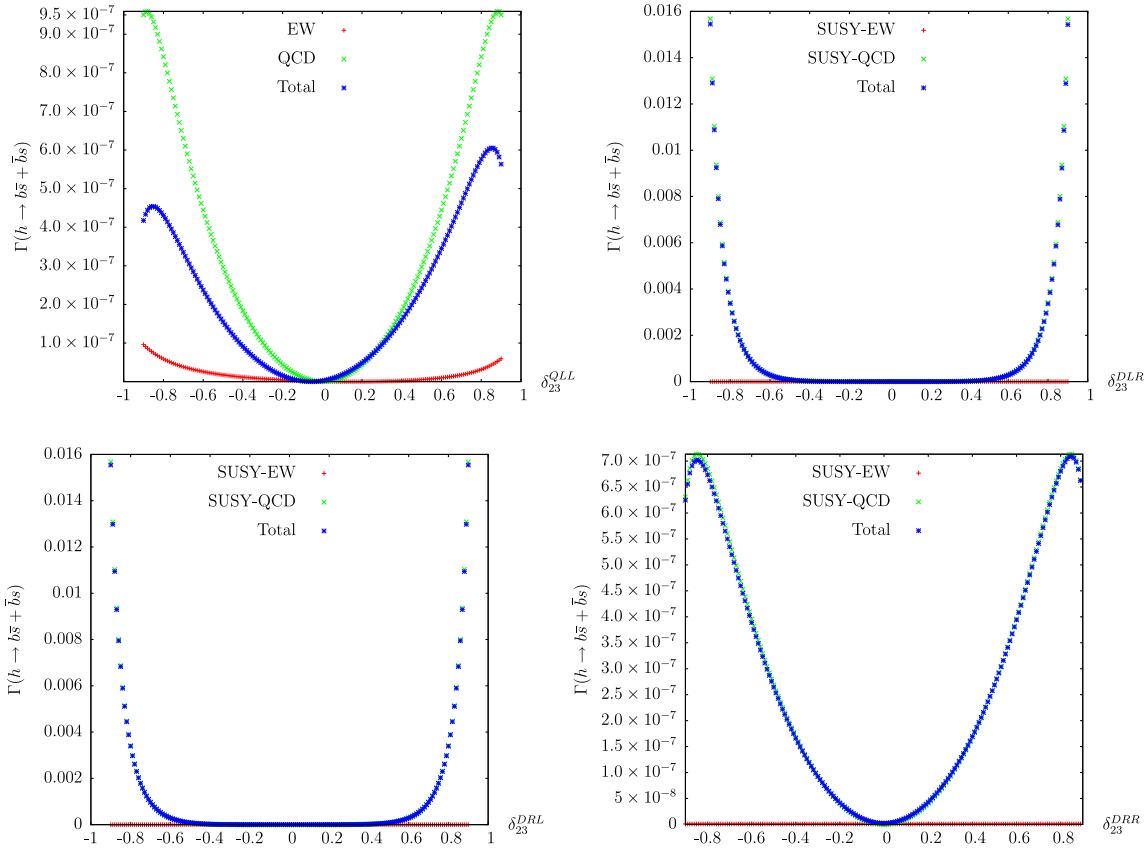

FIG. 4. $\Gamma(h \to \bar{b}s + b\bar{s})$ as a function of δ_{23}^{QLL} (upper left), δ_{23}^{DLR} (upper right), δ_{23}^{DRL} (lower left), and δ_{23}^{DRR} (lower right).

the SUSY-EW contribution reach up to $\mathcal{O}(10^{-7})$, resulting in a total contribution "in between," due to the negative interference between the SUSY-EW and SUSY-QCD contribution. For LR and RL mixing, shown in the upper right and lower left plot, respectively, the SUSY-QCD contribution reach up to the maximum value of $\mathcal{O}(10^{-2})$, while the SUSY-EW contribution reach only up to $\mathcal{O}(10^{-7})$. In this case, the total contribution is almost equal to the SUSY-QCD contribution as SUSY-EW contribution (and thus the interference) is relatively negligible. The LR and RL contributions appear to be the same due to the symmetric structure of the flavor-conserving part of the mass matrix, which yields the symmetric effect. For RR mixing, shown in the lower right plot, the SUSY-EW contribution of $\mathcal{O}(10^{-10})$ is again negligible compared to the SUSY-QCD contribution of $\mathcal{O}(10^{-7})$.

The apparent independence of the decay width on the sign of the δ_{ij}^{FAB}, in particular for the QCD corrections, is due to the fact that the amplitude is governed by one of the δ_{ij}^{FAB}; i.e., all relevant contributing diagrams are $\propto \delta_{ij}^{FAB}$. In this case, the decay width contains $|\delta_{ij}^{FAB}|^2$, and the sign dependence disappears. As the EW corrections are included, the simple analytical dependence is no longer valid; i.e., some relevant diagrams are not $\propto \delta_{ij}^{FAB}$, and the result becomes asymmetric, as can be seen in the upper left plot of Fig. 4. Since the EW corrections are only relevant for the LL mixing, in the other plots the result appears symmetric in the sign of δ_{ij}^{FAB}.

Now we turn to realistic scenarios that are in agreement with experimental data from BPO and EWPO. The starting points are the scenarios S1…S6 defined in Table II, where we vary the flavor violating δ_{ij}^{FAB} within the experimentally allowed ranges following the results given in Tables III and IV. We start with the scenarios in which we allow one of the δ_{ij}^{FAB} to be varied, while the others are set to zero. In Fig. 5, we show $\mathrm{BR}(h \to \bar{b}s + b\bar{s})$ as a function of δ_{23}^{QLL} (upper left), δ_{23}^{DLR} (upper right), δ_{23}^{DRL} (lower left) and δ_{23}^{DRR} (lower right), i.e. for the same set of δ_{ij}^{FAB} that has been analyzed in Fig. 4. It can be seen that allowing only one $\delta_{ij}^{FAB} \neq 0$ results in rather small values of $\mathrm{BR}(h \to \bar{b}s + b\bar{s})$. LL (upper left) and RL (lower left plot) mixing results in $\mathcal{O}(10^{-7})$ values for $\mathrm{BR}(h \to \bar{b}s + b\bar{s})$. One order of magnitude can be gained in the RR-mixing case (lower right). The largest values of $\mathrm{BR}(h \to \bar{b}s + b\bar{s})$ are obtained in the case of $\delta_{23}^{DLR} \neq 0$ (upper right plot). Here in S4 and S5 values of $\mathrm{BR}(h \to \bar{b}s + b\bar{s}) \sim 2 \times 10^{-4}$ can be found, possibly in the reach of future e^+e^- colliders; see Sec. III A.

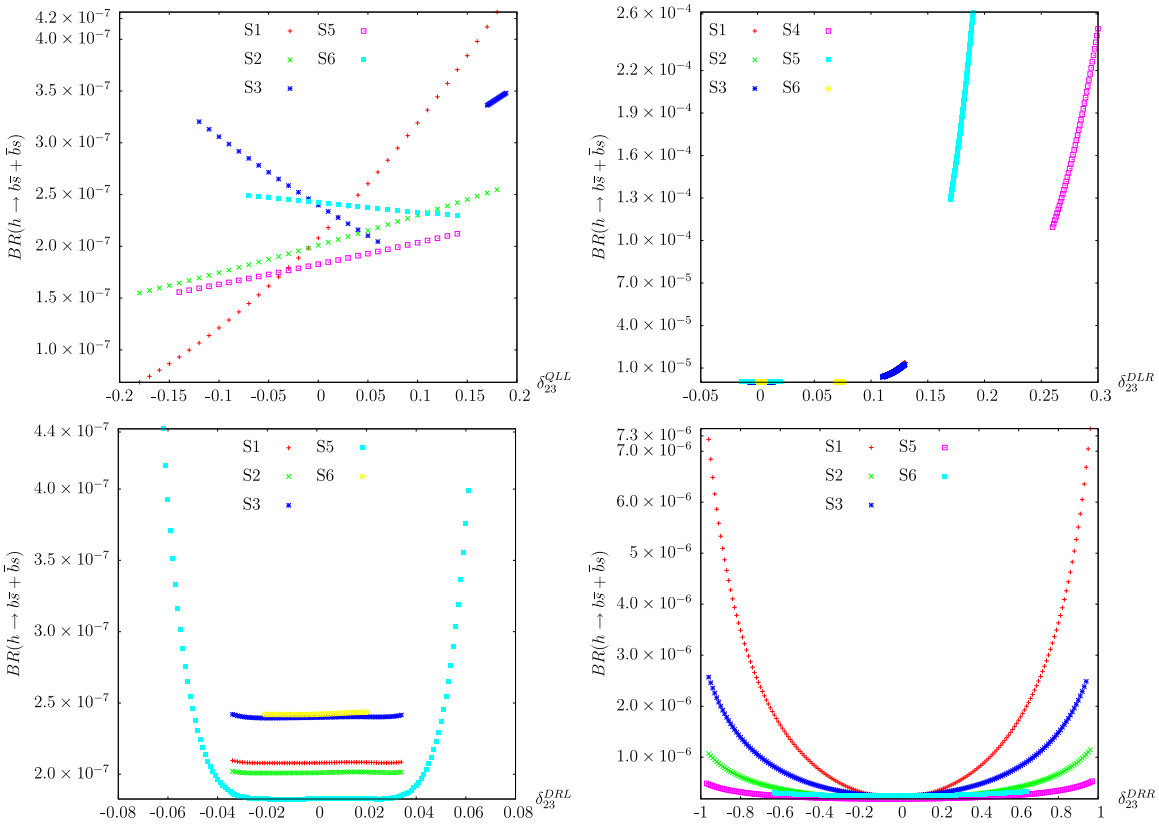

FIG. 5. $\mathrm{BR}(h \to \bar{b}s + b\bar{s})$ as a function of δ_{23}^{QLL} (upper left), δ_{23}^{DLR} (upper right), δ_{23}^{DRL} (lower left) and δ_{23}^{DRR} (lower right).

So far we have shown the effects of independent variations of one δ_{ij}^{FAB}. Obviously, a realistic model would include several $\delta_{ij}^{FAB} \neq 0$ that may interfere, increasing or decreasing the results obtained with just the addition of independent contributions. GUT based MFV models that induce the flavor violation via RGE running automatically generate several $\delta_{ij}^{FAB} \neq 0$ at the EW scale. In the following, we will present results with two or three $\delta_{ij}^{FAB} \neq 0$, where we combined the ones that showed the largest effects.

In Figs. 6–9, in the left columns we show the 3σ contours (with experimental and theory uncertainties added linearly) of $\mathrm{BR}(B \to X_s\gamma)$ (Black), $\mathrm{BR}(B_s \to \mu^+\mu^-)$ (Green), ΔM_{B_s} (Blue) and M_W (Red). For nonvisible contours, the whole plane is allowed by that constraint. The right columns show, for the same parameters, the results for $\mathrm{BR}(h \to \bar{b}s + b\bar{s})$. In Figs. 6 and 7, we present the results for the plane (δ_{23}^{QLL}, δ_{23}^{DLR}) for S1…S3 and for S4…S6, respectively. Similarly, in Figs. 8 and 9 we show the (δ_{23}^{DRR}, δ_{23}^{DLR}) plane. The shaded areas in all plots indicates the parameter space that is allowed by all experimental constraints. In the (δ_{23}^{QLL}, δ_{23}^{DLR}) planes, one can see that the large values for δ_{23}^{QLL} are not allowed by M_W, on the other hand, $\mathrm{BR}(B \to X_s\gamma)$ mostly restricts the value of δ_{23}^{DLR}. The largest values for $\mathrm{BR}(h \to \bar{b}s + b\bar{s})$ in each plane in the area allowed by the BPO and the EWPO are summarized in the upper part of Table V. One can see that in most cases we find $\mathrm{BR}(h \to \bar{b}s + b\bar{s}) \sim \mathcal{O}(10^{-5})$, which would render the observation difficult at current and future colliders. However, in the (δ_{23}^{QLL}, δ_{23}^{DLR}) plane in the scenarios S4 and S5, maximum values of $\mathcal{O}(3 \times 10^{-4})$ can be observed, which could be detectable at future ILC measurements. In the (δ_{23}^{DRR}, δ_{23}^{DLR}) plane, for these two scenarios even values of $\mathcal{O}(10^{-3})$ are reached, which would make a measurement of the flavor violating Higgs decay relatively easy at the ILC. These examples show that an experimental analysis about the detectability of $h \to \bar{b}s + b\bar{s}$ at the ILC would be very desirable.

As a last step in the model-independent analysis, we consider the case of three $\delta_{ij}^{FAB} \neq 0$ at a time. For this purpose, we scan the parameters in the (δ_{23}^{QLL}, δ_{23}^{DLR}) plane and set $\delta_{23}^{DRR} = 0.5$. For reasons of practicability, we choose *one* intermediate value for δ_{23}^{DRR}; a very small value will have no additional effect, and a very large value of δ_{23}^{DRR} leads to large excluded areas in the (δ_{23}^{QLL}, δ_{23}^{DLR}) plane. We show our results in Figs. 10 and 11 in the scenarios S1-S3 and S4-S6, respectively. Colors and shadings are chosen as in the previous analysis. Here it should be noted that in S4 the whole plane is excluded by M_W, and in S5 by $\mathrm{BR}(B_s \to \mu^+\mu^-)$ (both contours are not visible). In S6, no overlap between the four constraints is

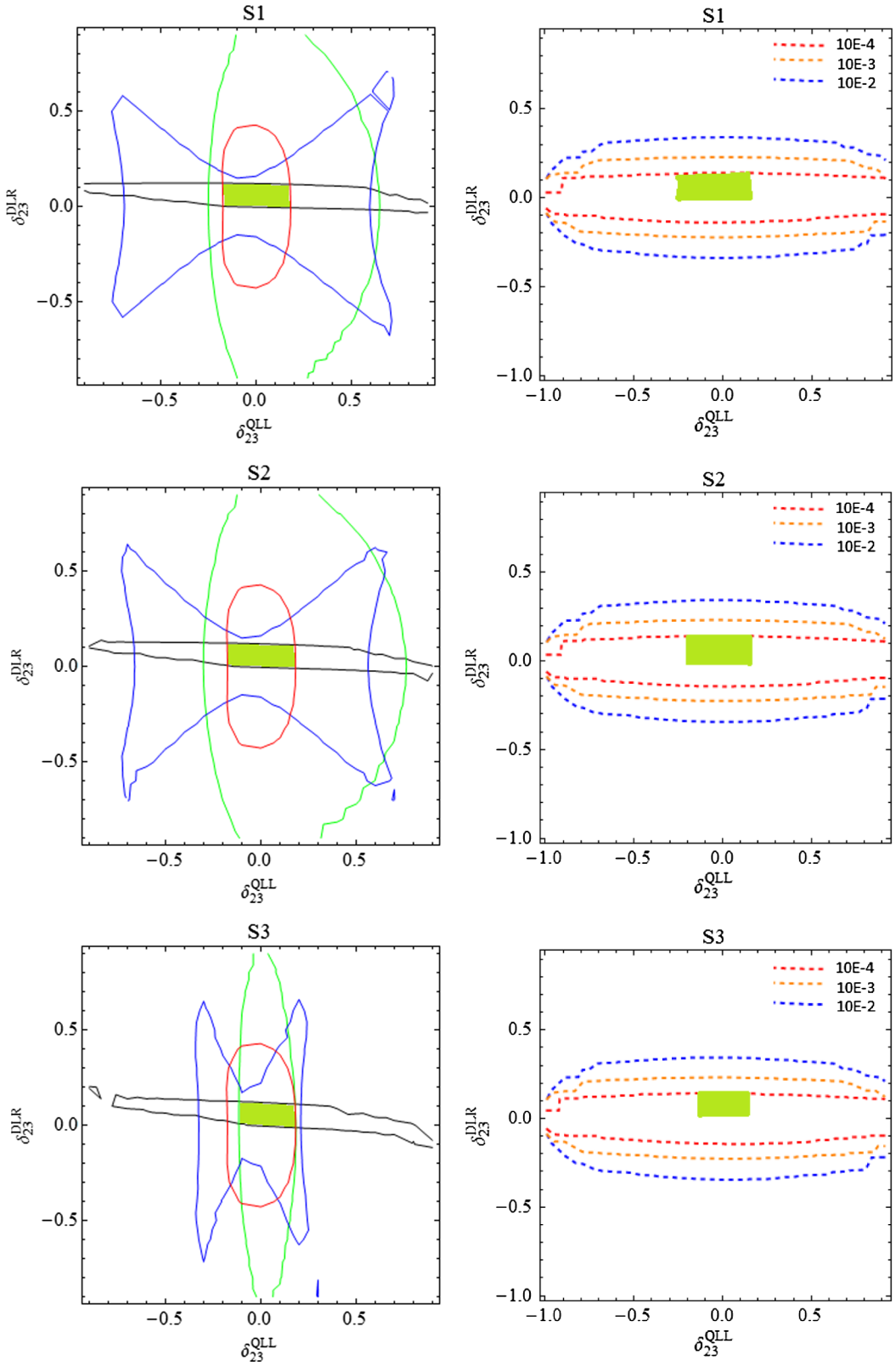

FIG. 6. Left: Contours of BR$(B \to X_s\gamma)$ (Black), BR$(B_s \to \mu^+\mu^-)$ (Green), ΔM_{B_s} (Blue) and M_W (Red) in $(\delta_{23}^{QLL}, \delta_{23}^{DLR})$ plane for points S1-S3. The shaded area shows the range of values allowed by all constraints. Right: corresponding contours for BR$(h \to \bar{b}s + b\bar{s})$.

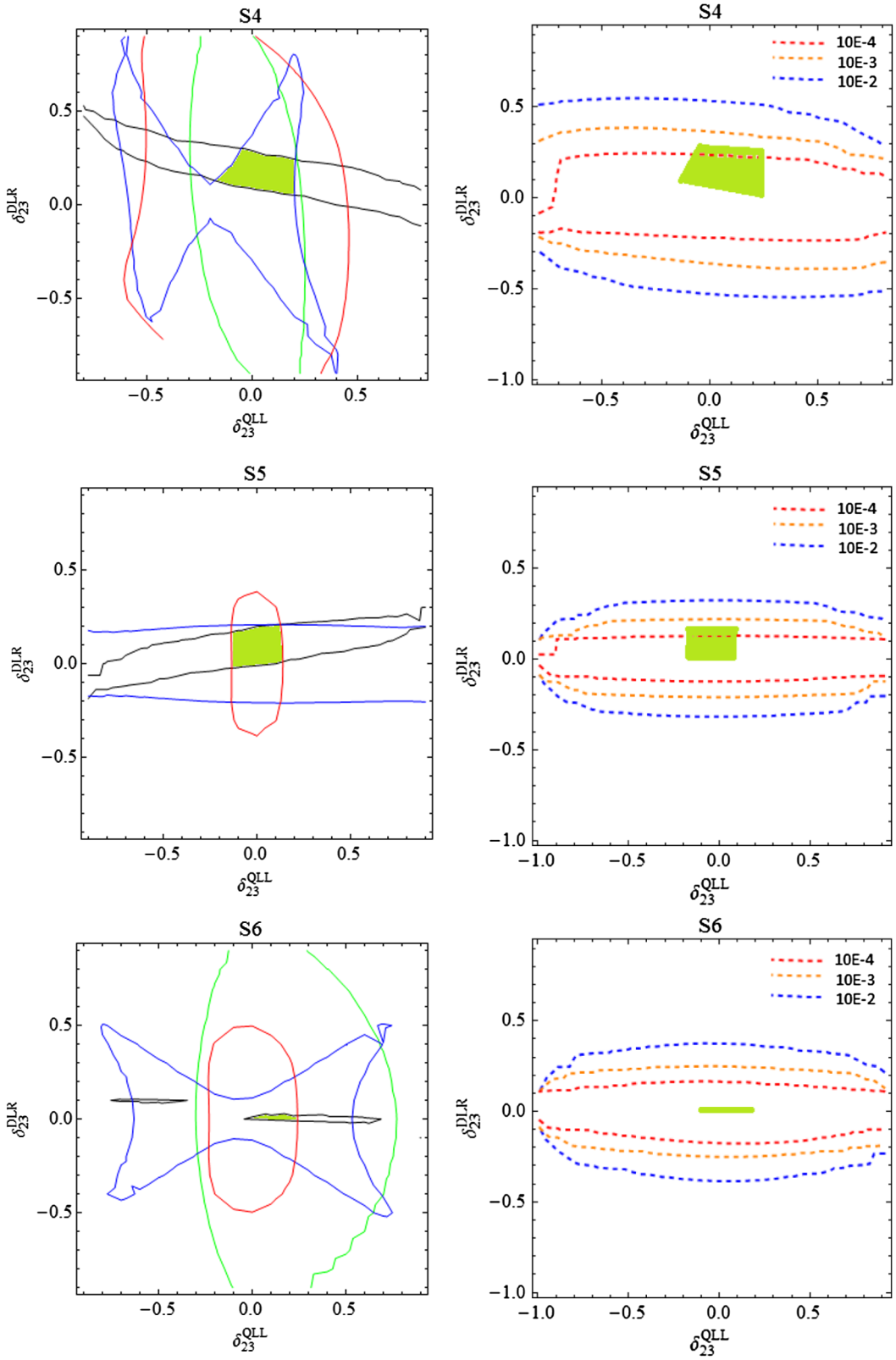

FIG. 7. Left: Contours of BR$(B \to X_s\gamma)$ (Black), BR$(B_s \to \mu^+\mu^-)$ (Green), ΔM_{B_s} (Blue) and M_W (Red) in $(\delta_{23}^{QLL}, \delta_{23}^{DLR})$ plane for points S4-S6. The shaded area shows the range of values allowed by all constraints. Right: corresponding contours for BR$(h \to \bar{b}s + b\bar{s})$.

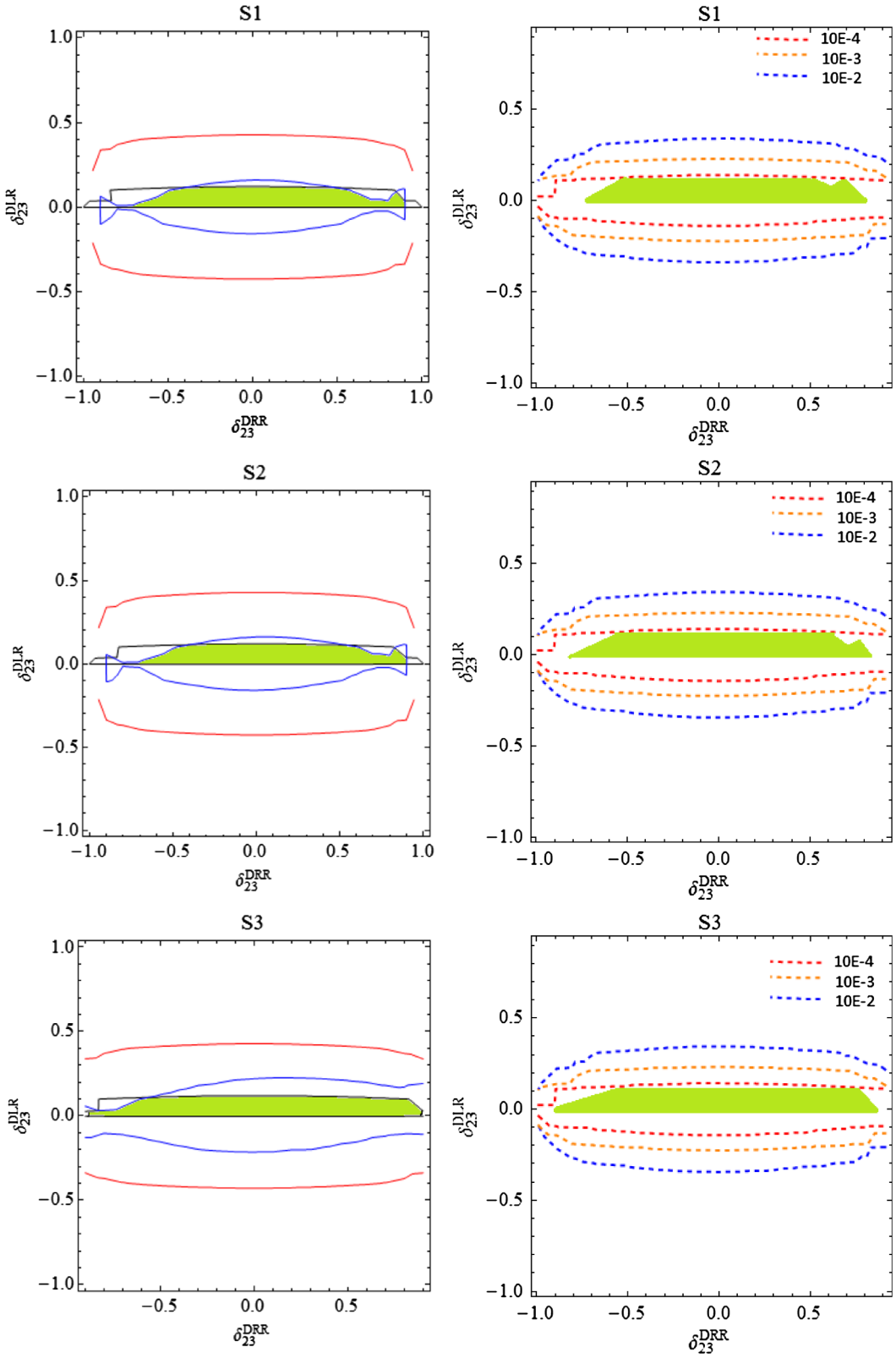

FIG. 8. Left: Contours of BR$(B \to X_s\gamma)$ (Black), BR$(B_s \to \mu^+\mu^-)$ (Green), ΔM_{B_s} (Blue) and M_W (Red) in $(\delta_{23}^{DRR}, \delta_{23}^{DLR})$ plane for points S1-S3. The shaded area shows the range of values allowed by all constraints. Right: corresponding contours for BR$(h \to \bar{b}s + b\bar{s})$.

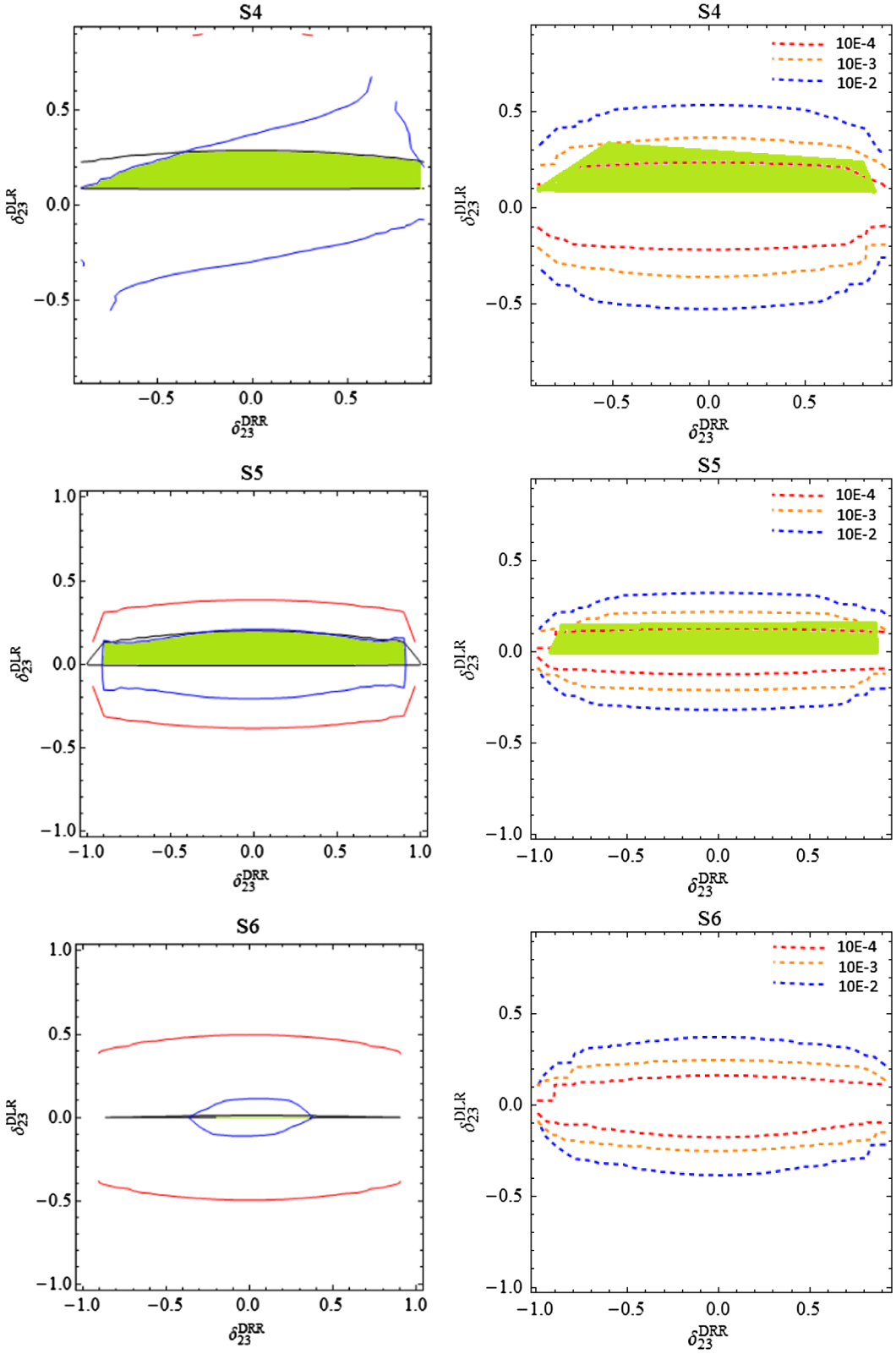

FIG. 9. Left: Contours of BR$(B \to X_s\gamma)$ (Black), BR$(B_s \to \mu^+\mu^-)$ (Green), ΔM_{B_s} (Blue) and M_W (Red) in $(\delta_{23}^{DRR}, \delta_{23}^{DLR})$ plane for points S4-S6. The shaded area shows the range of values allowed by all constraints. Right: corresponding contours for BR$(h \to \bar{b}s + b\bar{s})$.

TABLE V. Maximum possible value for $\mathrm{BR}(h \to \bar{b}s + b\bar{s})$ for two and three $\delta_{ij}^{FAB} \neq 0$ case for the selected S1-S6 MSSM points defined in Table II.

Plane	MSSM point	Maximum possible value	Figure
$(\delta_{23}^{QLL}, \delta_{23}^{DLR})$	S1	1.38×10^{-5}	Fig. 6
	S2	1.39×10^{-5}	Fig. 6
	S3	1.43×10^{-5}	Fig. 6
	S4	3.34×10^{-4}	Fig. 7
	S5	2.74×10^{-4}	Fig. 7
	S6	1.36×10^{-8}	Fig. 7
$(\delta_{23}^{DRR}, \delta_{23}^{DLR})$	S1	4.41×10^{-6}	Fig. 8
	S2	3.32×10^{-6}	Fig. 8
	S3	3.07×10^{-5}	Fig. 8
	S4	1.66×10^{-3}	Fig. 9
	S5	1.97×10^{-3}	Fig. 9
	S6	6.03×10^{-8}	Fig. 9
$(\delta_{23}^{QLL}, \delta_{23}^{DLR})$ with $\delta_{23}^{DRR} = 0.5$	S1	7.49×10^{-6}	Fig. 10
	S2	7.33×10^{-6}	Fig. 10
	S3	3.50×10^{-6}	Fig. 10
	S4	Excluded	Fig. 11
	S5	Excluded	Fig. 11
	S6	Excluded	Fig. 11

found, and again this scenario is excluded. We have checked that also a smaller value of $\delta_{23}^{DRR} = 0.2$ does not qualitatively change the picture for S4, S5 and S6. The highest values that can be reached for $\mathrm{BR}(h \to \bar{b}s + b\bar{s})$ in the three remaining scenarios in the experimentally allowed regions are shown in the lower part of Table V. One can see only very small values or $\mathcal{O}(5 \times 10^{-6})$ are found; i.e., choosing $\delta_{23}^{DRR} \neq 0$ did not lead to observable values of $\mathrm{BR}(h \to \bar{b}s + b\bar{s})$.

To summarize, in our model-independent analysis, allowing for more than one $\delta_{ij}^{FAB} \neq 0$, we find that the additional freedom resulted in somewhat larger values of $\mathrm{BR}(h \to \bar{b}s + b\bar{s})$ as compared to the case of only one nonzero δ_{ij}^{FAB}. In particular, in the two scenarios S4 and S5 values of $\mathrm{BR}(h \to \bar{b}s + b\bar{s}) \sim 10^{-3}$–$10^{-4}$ can be reached, allowing the detection of the flavor violating Higgs decay at the ILC. The other scenarios always yield values that are presumably too low for current and future colliders.

B. Numerical results in MFV CMSSM

In this final step of our numerical analysis, we investigate the CMSSM as described in Sec. II B. Here the MFV hypothesis is realized by demanding no flavor violation at the GUT scale, and the various flavor violating δ_{ij}^{FAB} are induced by the RGE running to the EW scale. For this analysis, the SUSY spectra have been generated with the code SPheno 3.2.4 [55]. We started with the definition of the (MFV) SLHA file [56] at the GUT scale. In a first step within SPheno, gauge and Yukawa couplings at the M_Z scale are calculated using tree-level formulas. Fermion masses, the Z boson pole mass, the fine structure constant α, the Fermi constant G_F and the strong coupling constant $\alpha_s(M_Z)$ are used as input parameters. The gauge and Yukawa couplings, calculated at M_Z, are then used as input for the one-loop RGEs to obtain the corresponding values at the GUT scale which is calculated from the requirement that $g_1 = g_2$ (where $g_{1,2}$ denote the gauge couplings of the $U(1)$ and $SU(2)$, respectively). The CMSSM boundary conditions (with the numerical values from the SLHA file) are then applied to the complete set of two-loop RGEs and are evolved to the EW scale. At this point the SM and SUSY radiative corrections are applied to the gauge and Yukawa couplings, and the two-loop RGEs are again evolved to GUT scale. After applying the CMSSM boundary conditions again the two-loop RGEs are run down to EW scale to get SUSY spectrum. This procedure is iterated until the required precision is achieved. The output is given in the form of an SLHA, file which is used as input for FeynHiggs to calculate low-energy observables discussed above.

In order to get an overview about the size of the effects in the CMSSM parameter space, the relevant parameters m_0, $m_{1/2}$ have been scanned as, or in case of A_0 and $\tan\beta$ have been set to all combinations of

$$\begin{aligned} m_0 &= 500\ \mathrm{GeV}\ldots5000\ \mathrm{GeV}, \\ m_{1/2} &= 1000\ \mathrm{GeV}\ldots3000\ \mathrm{GeV}, \\ A_0 &= -3000, -2000, -1000, 0\ \mathrm{GeV}, \\ \tan\beta &= 10, 20, 35, 45, \end{aligned} \tag{26}$$

with $\mu > 0$.

The results are shown in Fig. 12, where we display the contours of $\mathrm{BR}(h \to \bar{b}s + b\bar{s})$ in the $(m_0, m_{1/2})$ plane for $\tan\beta = 10$, $A_0 = 0$ (upper left), $\tan\beta = 10$, $A_0 = -3000$ GeV (upper right), $\tan\beta = 45$, $A_0 = 0$ (lower left) and $\tan\beta = 45$, $A_0 = -3000$ GeV (lower right). By comparison with planes for other $\tan\beta - A_0$ combinations we have verified that these four planes constitute a representative example. The allowed parameter space can be deduced by comparing to the results presented in Refs. [15,57]. While not all the planes are in agreement with current constraints, large parts, in particular for larger values of m_0 and $m_{1/2}$ are compatible with a combination of direct searches, flavor and electroweak precision observables as well as astrophysical data. Upper bounds on m_0 at the few TeV level could possibly be set by including the findings of Ref. [15] into a global CMSSM analysis.

In Fig. 12, one can see that for most of the parameter space, values of $\mathcal{O}(10^{-7})$ are found for $\mathrm{BR}(h \to \bar{b}s + b\bar{s})$, i.e. outside the reach of current or future collider experiments. Even for the "most extreme" set of parameters we have analyzed, $\tan\beta = 45$ and $A_0 = -3000$ GeV, no detectable rate has been found. Turning the argument

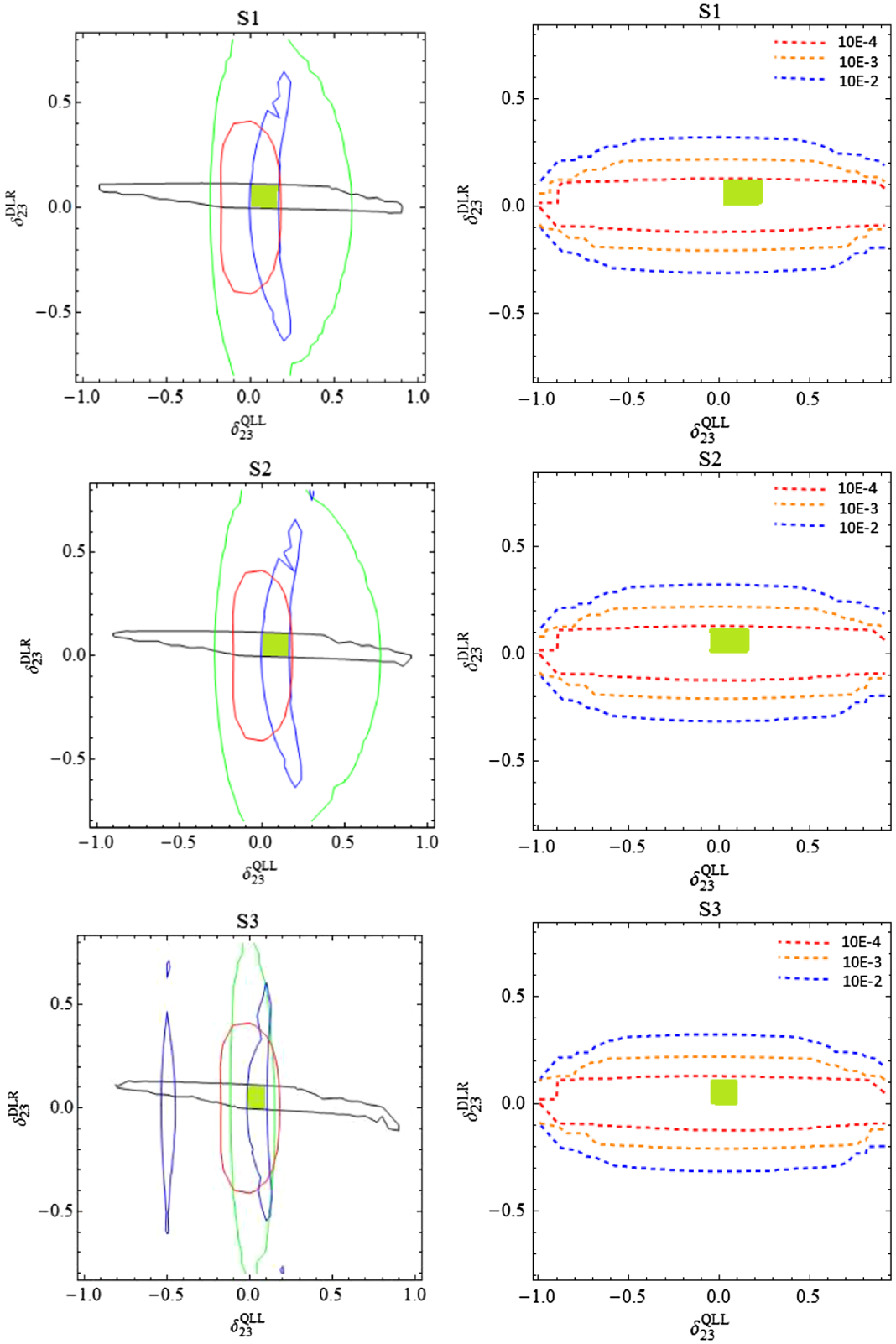

FIG. 10. Left: Contours of BR($B \to X_s\gamma$) (Black), BR($B_s \to \mu^+\mu^-$) (Green), ΔM_{B_s} (Blue) and M_W (Red) in the (δ_{23}^{QLL}, δ_{23}^{DLR}) plane with $\delta_{23}^{DRR} = 0.5$ for points S1-S3. The shaded area shows the range of values allowed by all constraints. Right: corresponding contours for BR($h \to \bar{b}s + b\bar{s}$).

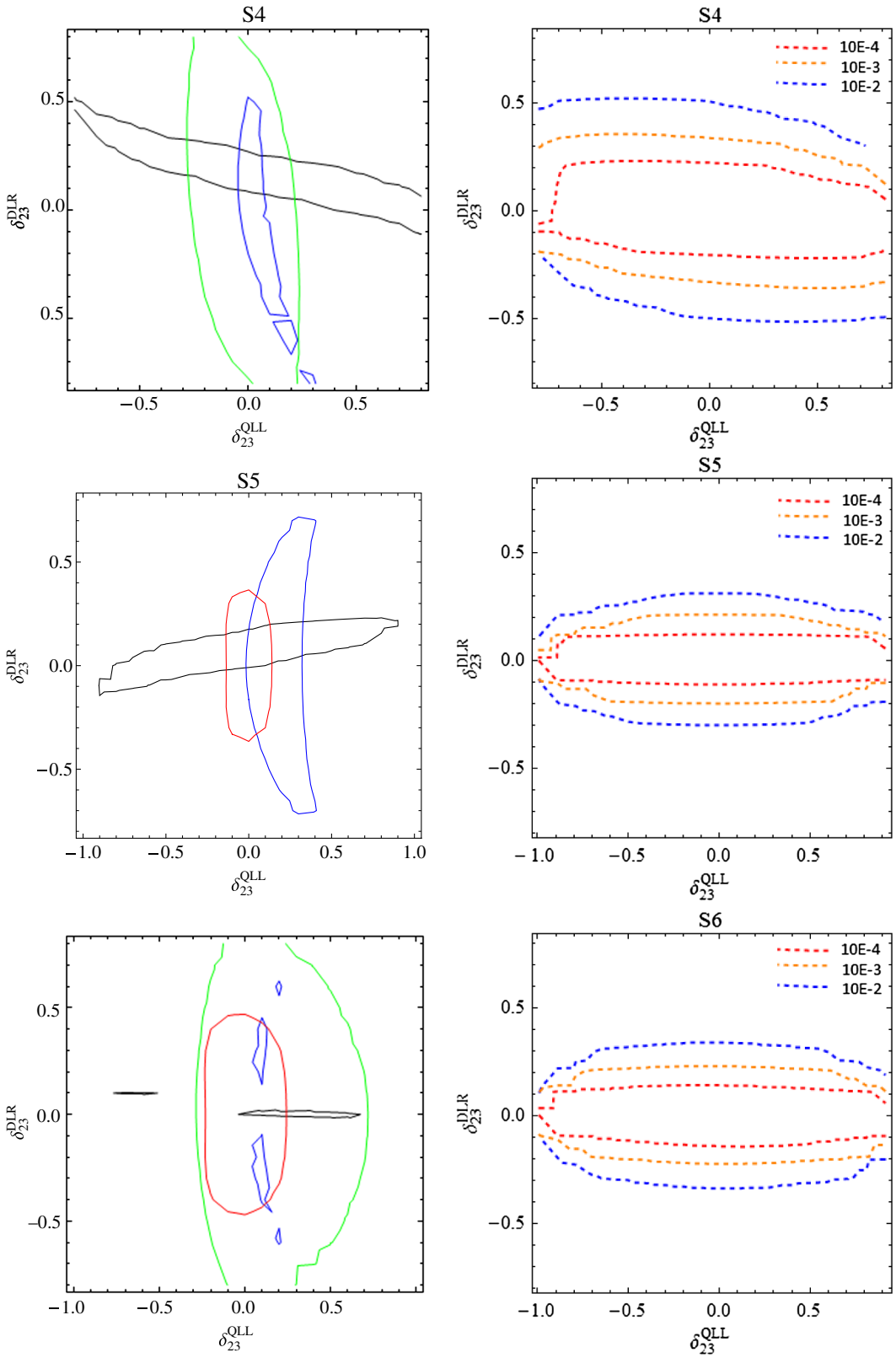

FIG. 11. Left: Contours of BR$(B \to X_s\gamma)$ (Black), BR$(B_s \to \mu^+\mu^-)$ (Green), ΔM_{B_s} (Blue) and M_W (Red) in the $(\delta_{23}^{QLL}, \delta_{23}^{DLR})$ plane with $\delta_{23}^{DRR} = 0.5$ for points S4-S6. The shaded area shows the range of values allowed by all constraints. Right: corresponding contours for BR$(h \to \bar{b}s + b\bar{s})$.

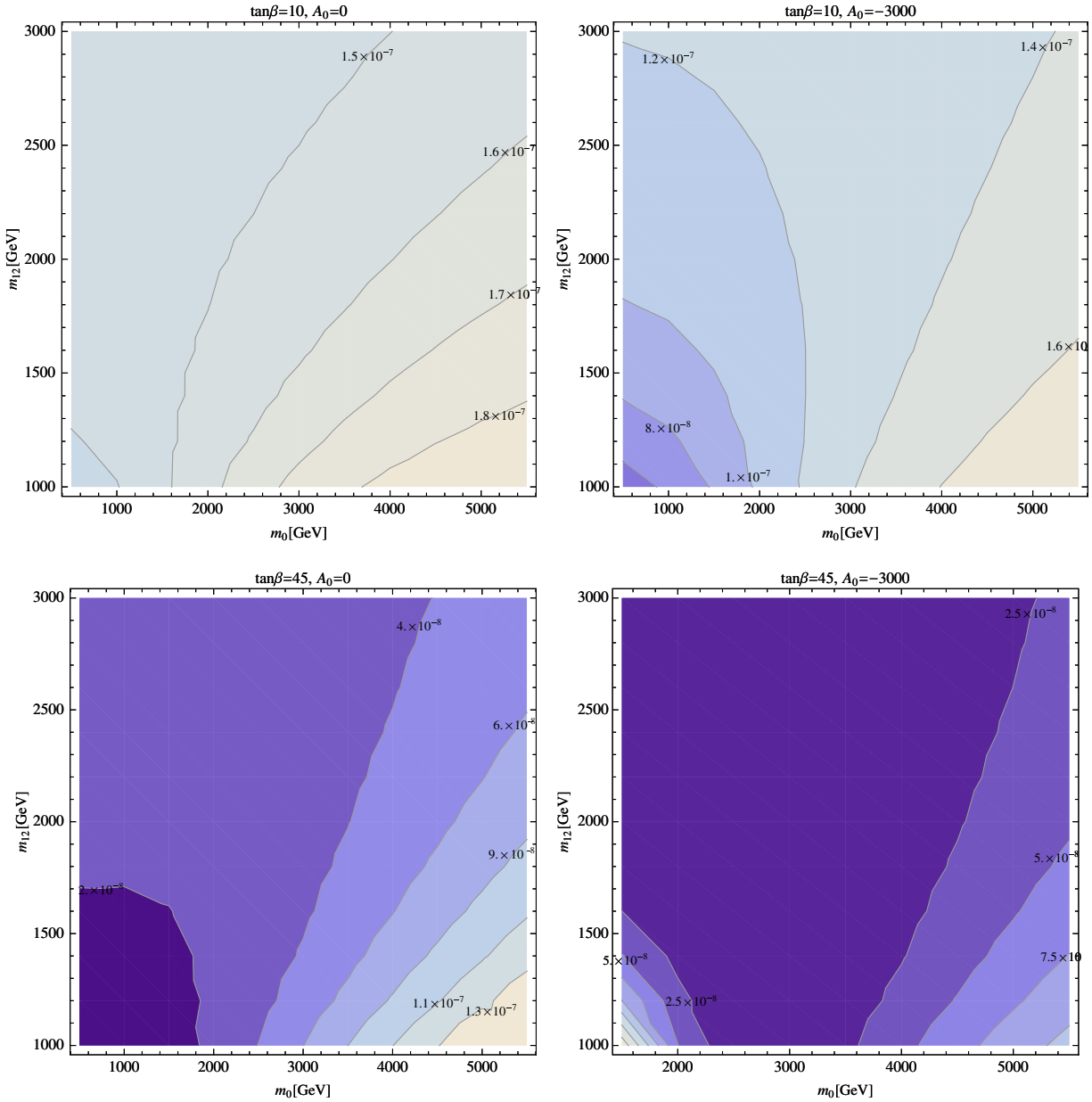

FIG. 12. Contours of BR$(h \to b\bar{s} + \bar{b}s)$ in the $(m_0, m_{1/2})$ plane for different values of $\tan\beta$ and A_0 in the CMSSM.

around, any observation of the decay $h \to \bar{b}s + b\bar{s}$ at the (discussed) future experiments would exclude the CMSSM as a possible model.

V. CONCLUSIONS

We have investigated the flavor violating Higgs boson decay $h \to \bar{b}s + b\bar{s}$ in the MSSM. This evaluation improves on existing analyses in various ways. We take into account the full set of SUSY QCD and SUSY EW corrections, allowing for LL, RL, LR, and RR mixing simultaneously. The parameter space is restricted not only by B-physics observables, but also by electroweak precision observables, in particular the mass of the W boson. Here we have shown that M_W can yield nontrivial, additional restrictions on the parameter space of the flavor violating δ_{ij}^{FAB}.

From the technical side we have (re)calculated the decay $h \to \bar{b}s + b\bar{s}$ in the FeynArts and FormCalc setup. The BPO and EWPO constraints have been evaluated with the help of (a private version of) FeynHiggs, taking into account the full flavor violating one-loop corrections to M_W and to the relevant B-physics observables (supplemented with further MSSM higher-order corrections). In the GUT-based models, the low-energy spectra have been evaluated with the help of SPheno.

The first part of the numerical analysis used a model-independent approach. In six representative scenarios, which are allowed by current searches for SUSY particles

and heavy Higgs bosons, we have evaluated the allowed parameter space for the various δ_{ij}^{FAB} by applying BPO and EWPO constraints. Within these allowed ranges, we have then evaluated $\mathrm{BR}(h \to \bar{b}s + b\bar{s})$. In the case of only one, $\delta_{ij}^{FAB} \neq 0$, we have found that only relatively large values of δ_{23}^{DLR} could lead to rates of $\mathrm{BR}(h \to \bar{b}s + b\bar{s}) \sim 10^{-4}$, which could be in the detectable range of future e^+e^- colliders. Allowing two $\delta_{ij}^{FAB} \neq 0$ simultaneously lead to larger values up to $\mathrm{BR}(h \to \bar{b}s + b\bar{s}) \sim 10^{-3}$, which would make the observation at the ILC relatively easy. Allowing for a third $\delta_{ij}^{FAB} \neq 0$, on the other hand, did not lead to larger values of the flavor violating branching ratio. We stress again, that no experimental analysis about the detectability of $h \to \bar{b}s + b\bar{s}$ at the ILC does not exist, but would be very desirable in view of our results.

In the final step of the numerical analysis, we have evaluated $\mathrm{BR}(h \to \bar{b}s + b\bar{s})$ in the MFV Constrained MSSM. In this model, the flavor violation is induced by CKM effects in the RGE running from the GUT to the EW scale. Here we have found that also for the "most extreme" set of parameters we have analyzed, $A_0 = -3000$ GeV and $\tan\beta = 45$, only negligible effects can be expected. Turning the argument around, detecting a nonzero value for $\mathrm{BR}(h \to \bar{b}s + b\bar{s})$ at (the discussed) future experiments would exclude the CMSSM as a viable model.

ACKNOWLEDGMENTS

The work of S. H. and M. R. was partially supported by CICYT (Grant No. FPA 2013-40715-P). M. G., S. H., and M. R. were supported by the Spanish MICINN's Consolider-Ingenio 2010 Programme under Grant No. MultiDark CSD2009-00064. M. E. G. acknowledges further support from the MICINN Projects No. FPA2011-23781 and No. FPA2014-53631-C2-2-P.

[1] S. Glashow, J. Iliopoulos, and L. Maiani, Phys. Rev. D **2**, 1285 (1970).
[2] H. Nilles, Phys. Rep. **110**, 1 (1984); H. Haber and G. Kane, Phys. Rep. **117**, 75 (1985); R. Barbieri, Riv. Nuovo Cimento **11**, 1 (1988).
[3] Y. Amhis *et al.* (Heavy Flavor Averaging Group), arXiv:1412.7515v1.
[4] R. Chivukula and H. Georgi, Phys. Lett. B **188**, 99 (1987); L. Hall and L. Randall, Phys. Rev. Lett. **65**, 2939 (1990); A. J. Buras, P. Gambino, M. Gorbahn, S. Jäger, and L. Silvestrini, Phys. Lett. B **500**, 161 (2001).
[5] G. D'Ambrosio, G. F. Giudice, G. Isidori, and A. Strumia, Nucl. Phys. **B645**, 155 (2002).
[6] S. Bejar, F. Dilme, J. Guasch, and J. Sola, J. High Energy Phys. 08 (2004) 018.
[7] A. Curiel, M. Herrero, and D. Temes, Phys. Rev. D **67**, 075008 (2003).
[8] D. Demir, Phys. Lett. B **571**, 193 (2003).
[9] A. Curiel, M. Herrero, W. Hollik, F. Merz, and S. Peñaranda, Phys. Rev. D **69**, 075009 (2004).
[10] G. Barenboim, C. Bosch, J. Lee, M. López-Ibáñez, and O. Vives, Phys. Rev. D **92**, 095017 (2015).
[11] M. Gómez, T. Hahn, S. Heinemeyer, and M. Rehman, Phys. Rev. D **90**, 074016 (2014).
[12] M. Arana-Catania, S. Heinemeyer, and M. Herrero, Phys. Rev. D **88**, 015026 (2013).
[13] M. Arana-Catania, S. Heinemeyer, M. Herrero, and S. Peñaranda, J. High Energy Phys. 05 (2012) 015; arXiv:1201.6345.
[14] M. Arana-Catania, S. Heinemeyer, and M. Herrero, Phys. Rev. D **90**, 075003 (2014).
[15] M. Gómez, S. Heinemeyer, and M. Rehman, Eur. Phys. J. C **75**, 434 (2015).
[16] B. Allanach *et al.*, Comput. Phys. Commun. **180**, 8 (2009).
[17] T. Ibrahim and P. Nath, Rev. Mod. Phys. **80**, 577 (2008).
[18] M. Pospelov and A. Ritz, Ann. Phys. (Amsterdam) **318**, 119 (2005).
[19] N. Falck, Z. Phys. C **30**, 247 (1986).
[20] S. Bertolini, F. Borzumati, A. Masiero, and G. Ridolfi, Nucl. Phys. **B353**, 591 (1991).
[21] J. Küblbeck, M. Böhm, and A. Denner, Comput. Phys. Commun. **60**, 165 (1990); T. Hahn, Comput. Phys. Commun. **140**, 418 (2001).
[22] T. Hahn and C. Schappacher, Comput. Phys. Commun. **143**, 54 (2002); The program and the user's guide are available at www.feynarts.de.
[23] T. Hahn and M. Pérez-Victoria, Comput. Phys. Commun. **118**, 153 (1999).
[24] S. Heinemeyer, W. Hollik, and G. Weiglein, Comput. Phys. Commun. **124**, 76 (2000); T. Hahn, S. Heinemeyer, W. Hollik, H. Rzehak, and G. Weiglein, Comput. Phys. Commun. **180**, 1426 (2009); see www.feynhiggs.de.
[25] S. Heinemeyer, W. Hollik, and G. Weiglein, Eur. Phys. J. C **9**, 343 (1999).
[26] G. Degrassi, S. Heinemeyer, W. Hollik, P. Slavich, and G. Weiglein, Eur. Phys. J. C **28**, 133 (2003).
[27] M. Frank, T. Hahn, S. Heinemeyer, W. Hollik, R. Rzehak, and G. Weiglein, J. High Energy Phys. 02 (2007) 047.
[28] T. Hahn, S. Heinemeyer, W. Hollik, H. Rzehak, and G. Weiglein, Phys. Rev. Lett. **112**, 141801 (2014).
[29] G. Moortgat-Pick *et al.*, Eur. Phys. J. C **75**, 371 (2015).
[30] G. Isidori and A. Retico, J. High Energy Phys. 09 (2002) 063.
[31] P. Chankowski and L. Slawianowska, Phys. Rev. D **63**, 054012 (2001).
[32] J. Foster, K. Okumura, and L. Roszkowski, J. High Energy Phys. 08 (2005) 094.

[33] G. Isidori and P. Paradisi, Phys. Lett. B **639**, 499 (2006); G. Isidori, F. Mescia, P. Paradisi, and D. Temes, Phys. Rev. D **75**, 115019 (2007) and references therein.
[34] See https://www.slac.stanford.edu/xorg/hfag/rare/2013/radll/OUTPUT/TABLES/radll.pdf.
[35] M. Misiak, Acta Phys. Pol. B **40**, 2987 (2009).
[36] S. Chatrchyan *et al.* (CMS Collaboration), Phys. Rev. Lett. **111**, 101804 (2013).
[37] R. Aaij *et al.* (LHCb Collaboration), Phys. Rev. Lett. **111**, 101805 (2013).
[38] A. Buras, J. Girrbach, D. Guadagnoli, and G. Isidori, Eur. Phys. J. C **72**, 2172 (2012).
[39] See https://www.slac.stanford.edu/xorg/hfag/osc/PDG_2013/.
[40] A. Buras, M. Jamin, and P. Weisz, Nucl. Phys. **B347**, 491 (1990).
[41] E. Golowich, J. Hewett, S. Pakvasa, A. Petrov, and G. Yeghiyan, Phys. Rev. D **83**, 114017 (2011).
[42] CMS and LHCb Collaborations, Reports No. CMS-PAS-BPH-13-007, No. LHCb-CONF-2013-012, and No. CERN-LHCb-CONF-2013-012.
[43] S. Heinemeyer, W. Hollik, and G. Weiglein, Phys. Rep. **425**, 265 (2006).
[44] S. Schael *et al.* (ALEPH, DELPHI, L3, OPAL and LEP Electroweak Collaborations), Phys. Rep. **532**, 119 (2013); see http://www.cern.ch/LEPEWWG.
[45] M. Baak *et al.*, arXiv:1310.6708; A. Freitas *et al.*, arXiv:1307.3962.
[46] S. Heinemeyer, in Proceedings of 8th FCC-ee Physics Workshop, Paris, France, October 2014, https://indico.cern.ch/event/337673/session/3/contribution/41/material/slides.
[47] M. Veltman, Nucl. Phys. **B123**, 89 (1977).
[48] S. Heinemeyer, W. Hollik, F. Merz, and S. Peñaranda, Eur. Phys. J. C **37**, 481 (2004).
[49] A. Djouadi, P. Gambino, S. Heinemeyer, W. Hollik, C. Jünger, and G. Weiglein, Phys. Rev. Lett. **78**, 3626 (1997); Phys. Rev. D **57**, 4179 (1998).
[50] S. Heinemeyer, W. Hollik, D. Stöckinger, A. Weber, and G. Weiglein, J. High Energy Phys. 08 (2006) 052.
[51] J. Haestier, S. Heinemeyer, D. Stöckinger, and G. Weiglein, J. High Energy Phys. 12 (2005) 027.
[52] H. Haber and Y. Nir, Nucl. Phys. **B335**, 363 (1990).
[53] M. Dührssen, in Proceedings of Rencontres de Moriond EW 2015, https://indico.in2p3.fr/event/10819/session/3/contribution/102/material/slides/1.pdf.
[54] P. Bechtle, O. Brein, S. Heinemeyer, G. Weiglein, and K. Williams, Comput. Phys. Commun. **181**, 138 (2010); **182**, 2605 (2011); P. Bechtle, O. Brein, S. Heinemeyer, O. Stål, T. Stefaniak, G. Weiglein, and K. Williams, Eur. Phys. J. C **74**, 2693 (2014).
[55] W. Porod, Comput. Phys. Commun. **153**, 275 (2003); W. Porod and F. Staub, Comput. Phys. Commun. **183**, 2458 (2012).
[56] P. Skands *et al.*, J. High Energy Phys. 07 (2004) 036; B. Allanach *et al.*, Comput. Phys. Commun. **180**, 8 (2009).
[57] O. Buchmueller *et al.*, Eur. Phys. J. C **74**, 2922 (2014); **75**, 500 (2015).